AGU PUBLICATIONS

JGR

Journal of Geophysical Research: Atmospheres

RESEARCH ARTICLE
10.1002/2016JD024863

Key Points:
- A full year of global reanalysis of CO is evaluated and investigated
- Assimilation reveals larger role of hydrocarbon oxidation in the CO burden
- Model CH_4 lifetime improvement with CO reanalysis points to uncertainties in nonlinear processes

Supporting Information:
- Supporting Information S1

Correspondence to:
B. Gaubert,
gaubert@ucar.edu

Citation:
Gaubert, B., et al. (2016), Toward a chemical reanalysis in a coupled chemistry-climate model: An evaluation of MOPITT CO assimilation and its impact on tropospheric composition, *J. Geophys. Res. Atmos., 121*, 7310–7343, doi:10.1002/2016JD024863.

Received 26 JAN 2016
Accepted 25 MAY 2016
Accepted article online 28 MAY 2016
Published online 18 JUN 2016

Toward a chemical reanalysis in a coupled chemistry-climate model: An evaluation of MOPITT CO assimilation and its impact on tropospheric composition

B. Gaubert[1], A. F. Arellano Jr.[2], J. Barré[1], H. M. Worden[1], L. K. Emmons[1], S. Tilmes[1], R. R. Buchholz[1], F. Vitt[1], K. Raeder[3], N. Collins[3], J. L. Anderson[3], C. Wiedinmyer[1], S. Martinez Alonso[1], D. P. Edwards[1], M. O. Andreae[4], J. W. Hannigan[1], C. Petri[5], K. Strong[6], and N. Jones[7]

[1]National Center for Atmospheric Research, Atmospheric Chemistry Observations and Modeling Laboratory, Boulder, Colorado, USA, [2]Department of Atmospheric Sciences, University of Arizona, Tucson, Arizona, USA, [3]National Center for Atmospheric Research, Institute for Mathematics Applied to Geosciences, Boulder, Colorado, USA, [4]Biogeochemistry Department, Max Planck Institute for Chemistry, Mainz, Germany, [5]Institute of Environmental Physics (IUP), University of Bremen, Bremen, Germany, [6]Department of Physics, University of Toronto, Toronto, Ontario, Canada, [7]University of Wollongong, Wollongong, New South Wales, Australia

Abstract We examine in detail a 1 year global reanalysis of carbon monoxide (CO) that is based on joint assimilation of conventional meteorological observations and Measurement of Pollution in The Troposphere (MOPITT) multispectral CO retrievals in the Community Earth System Model (CESM). Our focus is to assess the impact to the chemical system when CO distribution is constrained in a coupled full chemistry-climate model like CESM. To do this, we first evaluate the joint reanalysis (MOPITT Reanalysis) against four sets of independent observations and compare its performance against a reanalysis with no MOPITT assimilation (Control Run). We then investigate the CO burden and chemical response with the aid of tagged sectoral CO tracers. We estimate the total tropospheric CO burden in 2002 (from ensemble mean and spread) to be 371 ± 12% Tg for MOPITT Reanalysis and 291 ± 9% Tg for Control Run. Our multispecies analysis of this difference suggests that (a) direct emissions of CO and hydrocarbons are too low in the inventory used in this study and (b) chemical oxidation, transport, and deposition processes are not accurately and consistently represented in the model. Increases in CO led to net reduction of OH and subsequent longer lifetime of CH_4 (Control Run: 8.7 years versus MOPITT Reanalysis: 9.3 years). Yet at the same time, this increase led to 5–10% enhancement of Northern Hemisphere O_3 and overall photochemical activity via HO_x recycling. Such nonlinear effects further complicate the attribution to uncertainties in direct emissions alone. This has implications to chemistry-climate modeling and inversion studies of longer-lived species.

1. Introduction

Oxidation in the troposphere is mainly controlled by the hydroxyl radical (OH), which initiates a complex chain of reactions that significantly affects the abundance of radiatively and chemically important species such as ozone (O_3), methane (CH_4), and secondary organic aerosols [*Isaksen et al.*, 2009]. For example, the OH radical reacts with atmospheric CH_4, nonmethane volatile organic compounds (NMVOCs), and carbon monoxide (CO), leading to the ultimate oxidation of reduced carbon in the troposphere to carbon dioxide (CO_2). The reaction with CO is considered the primary chemical loss mechanism for OH, followed by its reaction with CH_4 [*Levy*, 1971]. Changes in CO and CH_4 abundance therefore introduce important perturbations in the chemical system of the troposphere, resulting in changes in radiative forcing from these species [*Stocker et al.*, 2013]. Larger emissions of CO, in particular, lead to increases in the burden of several tropospheric species due to the reduction in OH [*Prather*, 1996]. The subsequent increase in CH_4 burden (and its lifetime) leads to a positive feedback on CO abundance through chemical production of CO from CH_4 [*Guthrie*, 1989]. Furthermore, at appropriate levels of nitrogen oxides ($NO_x = NO_2 + NO$), the CO + OH reaction is also efficiently involved in the photochemical production of tropospheric O_3 [*Crutzen*, 1973; *Logan et al.*, 1981]. The efficiency of O_3 production and the chemical oxidation of CH_4 and CO are controlled by the recycling of the HO_x family of radicals, consisting of OH, hydroperoxy (HO_2), organic peroxy (RO_2), and oxy (RO) radicals. Constraints on the interdependence between CO, CH_4 (and NMVOCs), and OH are therefore critical in understanding the overall chemical response to perturbations in tropospheric composition and associated climate forcings.

1.1. Tropospheric CO Sources and Sinks

Carbon monoxide is directly emitted into the troposphere from incomplete combustion of carbonaceous materials. This includes fossil fuel and biofuel use in energy production, domestic heating, transportation, and manufacturing, as well as agricultural and natural fires. Globally, fossil fuel/biofuel (FFBF) combustion constitutes the main primary source of CO emissions. At present, it produces CO at a rate of about 500–600 Tg CO/yr [*Shindell et al*., 2006; *Duncan et al*., 2007; *Stein et al*., 2014], predominantly originating from industrialized regions like North America, Europe, and East Asia. Biomass burning (BB) contributes about 350–500 Tg CO/yr, mostly from tropical and boreal forest fires [*Andreae and Merlet*, 2001; *Duncan et al*., 2003; *Kaiser et al*., 2012]. BB sources show a stronger climate-related seasonal and interannual variation than FFBF. Consequently, it strongly drives the interannual variability of CO abundance [*Novelli et al*., 2003; *van der Werf et al*., 2006; *Edwards et al*., 2006b; *Hooghiemstra et al*., 2012; *Worden et al*., 2013]. For example, observational evidence shows that episodic large-scale fires, which emit significant amounts of CO [*Pfister et al*., 2005; *Krol et al*., 2013], are most likely influenced by the El Niño–Southern Oscillation or ENSO [*Edwards et al*., 2006a; *Logan et al*., 2008].

CO is also produced from chemical oxidation. This secondary source of CO is, in fact, larger than the FFBF or BB direct emissions. Around 800 Tg CO/yr is produced from CH_4 oxidation and about 600 Tg CO/yr from NMVOCs oxidation, which are mainly of biogenic origin and to a lesser extent from anthropogenic sources [*Granier et al*., 2000; *Prather et al*., 2001; *Shindell et al*., 2006; *Duncan et al*., 2007; *Stein et al*., 2014]. The CO seasonality is further complicated by biogenic emissions, which peak during the summer and may dominate when anthropogenic sources are low or have been drastically reduced in industrialized countries [*Hudman et al*., 2008]. However, recent studies tend to show an underestimation of anthropogenic VOC emissions [*Stein et al*., 2014; *Emmons et al*., 2015].

CO is mainly removed from the atmosphere through its reaction with OH and to a lesser extent by dry deposition and soil uptake. Globally, CO has an average lifetime of 2.3 months (assuming an average OH concentration of 1.1×10^6 molecule/cm^3). It varies seasonally and regionally from 1 month to 2.5 months depending on the distribution of OH. In any case, its lifetime is longer than characteristic hemispheric and tropospheric mixing time scales. This makes CO a good signature of combustion, which is useful in tracking long-range transport of pollution, in general, and BB plumes in particular [e.g., *Edwards et al*., 2004]. Furthermore, the relative abundance of CO and CO_2 in plumes provides a good indication of combustion efficiency making it useful to constrain emission factors [*Kondo et al*., 2011; *Silva et al*., 2013]. The abundance and spatiotemporal distribution of CO in the troposphere are driven by the interplay between its sources and sinks. While uncertainties regarding CO sources still exist, global multimodel (and single-model) simulations of tropospheric chemistry consistently show large differences even when using similar sources. This discrepancy is attributed to differences in the simulated OH distribution [*Duncan et al*., 2007; *Naik et al*., 2013; *Monks et al*., 2015; *Strode et al*., 2015], which leads us back to the CH_4-CO-OH conundrum and role of nonlinear chemistry in better understanding changes in climate forcing that are associated with changes in combustion-related emissions.

1.2. Constraints on Tropospheric CO From MOPITT

Despite these remaining uncertainties, our present understanding of the spatiotemporal distribution of CO and its variability has greatly improved in the past decade. This is largely due to the availability of aircraft measurements; thanks to the National Oceanic and Atmospheric Administration (NOAA) and the Measurement of Ozone and Water Vapor by Airbus In-Service Aircraft (MOZAIC) observational programs [e.g., *Novelli et al*., 1998, 2003; *Emmons et al*., 2004; *Nédélec et al*., 2003; *Zbinden et al*., 2013; *Novelli and Masarie*, 2015] and spaceborne measurements such as the Measurement of the Pollution in the Troposphere (MOPITT), the Atmospheric Infrared Sounder (AIRS), the Tropospheric Emissions Spectrometer (TES), and the Infrared Atmospheric Sounding Interferometer (IASI) [e.g., *Jones et al*., 2003; *Warner et al*., 2007; *Worden et al*., 2013, 2014; *Deeter et al*., 2014; *George et al*., 2015; *Clerbaux et al*., 2015]. Past studies have integrated these observations of CO and related gases in both regional and global chemical transport models to constrain sources and sinks, in particular CO emissions [*Streets et al*., 2013, and references therein]. These assimilation efforts have evolved from Bayesian synthesis inversions [e.g., *Palmer et al*., 2003; *Heald et al*., 2004; *Pétron et al*., 2004; *Arellano et al*., 2004; *Pfister et al*., 2005; *Arellano et al*., 2006; *Stavrakou and Muller*, 2006; *Jones et al*., 2009; *Konovalov et al*., 2011; *Kopacz et al*., 2010], variational methods [*Chevallier et al*., 2009; *Fortems-Cheiney et al*., 2009, 2011; *Hooghiemstra et al*., 2012; *Jiang et al*., 2011, 2013, 2015], and comparison

of these two approaches [*Kopacz et al*., 2009] to data assimilation (DA) frameworks [*Miyazaki et al*., 2012b, 2015] and multispecies inversions [*Muller and Stavrakou*, 2005; *Pison et al*., 2009; *Jiang et al*., 2011]. Most recent studies have also shown that (1) aggregating the NMVOC sources in a global background (CO from chemical oxidation) leads to an overestimate of CO sources [*Jiang et al*., 2011] and (2) systematic biases in emission estimates may be caused by (a) model errors such as vertical transport and convection [*Jiang et al*., 2013, 2015], (b) aggregating emission estimates to larger footprints, (c) errors in representing biogenic CO, and (d) specifying (prescribing) OH distribution [*Jiang et al*., 2015].

Different versions of MOPITT CO have previously been assimilated to constrain the CO atmospheric concentrations for chemical weather studies using variational and sequential DA methods [*Lamarque et al*., 2004; *Yudin et al*., 2004; *Pradier et al*., 2006; *Arellano et al*., 2007; *Barré et al*., 2013, 2015; *Klonecki et al*., 2012; *Inness et al*., 2013, 2015]. Furthermore, these studies have been extended by several groups to longer assimilation periods (i.e., reanalysis activities) to provide insights on decadal trends of CO distribution and emissions. This entailed more sophisticated analysis approaches, including better representation of chemical sources of CO and multiple observational constraints. For example, *Fortems-Cheiney et al*. [2011] presented results of 10 years of assimilation of MOPITT version 4 Thermal Infrared (TIR) retrievals using the LMDZ-SACS (Laboratoire de Météorologie Dynamique model with Zooming capability-Simplified Atmospheric Chemistry System) mechanism [*Chevallier et al*., 2009; *Pison et al*., 2009]. This mechanism represents the CH_4 oxidation chain by a few reactive species (CO, CH_4, HCHO, H_2, OH, and methyl-chloroform). Their system used a 4D-Var scheme that optimized OH, 3-D chemical sources of formaldehyde (HCHO), and CO surface emissions. The *Fortems-Cheiney et al*. [2011] study concluded that proper treatment of chemical sources of CO in conjunction with jointly constraining OH is important to produce accurate and consistent estimates of CO emissions. In the context of the European Monitoring Atmospheric Composition and Climate (MACC) project, which was followed by the Copernicus Atmosphere Monitoring Service (CAMS), a weakly coupled chemistry-meteorology 4D-Var data assimilation system has been developed at the European Center for Medium-Range Weather Forecast (ECMWF) [*Inness et al*., 2015]. *Inness et al*. [2013] presented an 8 year reanalysis of MOPITT TIR total column CO retrievals (as well as other satellite data sets including IASI CO) for which O_3, CO, and NO_x initial conditions were optimized based on the coupling between the Integrated Forecasting System (IFS) and the Model for Ozone and Related chemical Tracers (MOZART-3) chemistry transport model. More recently, *Miyazaki et al*. [2015] presented a full chemistry ensemble-based reanalysis of MOPITT TIR 700 hPa CO retrievals (and other satellite-derived measurements such as O_3 from TES, NO_2 from OMI, and HNO_3 from MLS) with optimization of CO emissions only. Neither reanalysis provided a detailed discussion of the CO budgets including estimates of the chemical CO sources, as had been done in *Fortems-Cheiney et al*. [2011, 2012] and *Yin et al*. [2015]. However, the latter studies used a simplified chemistry scheme within an offline chemistry transport model.

Finally, the recent studies of tropospheric CO summarized above point to a new direction of incorporating multiple observational constraints into current models of atmospheric chemistry. However, it still points to a gap in our understanding of the variability in CO atmospheric concentrations mostly associated with the coupled nonlinear nature of the factors controlling its abundance (see section 1.1). In particular, issues remain regarding the following: (a) accuracy and consistency of concentration and emission trends due to errors in model representation of transport, deposition, chemical production, and loss, which are not mutually exclusive, and (b) uncertainties in sectoral and regional emissions of CO and hydrocarbons. While recent studies have begun tackling some of these issues independently, detailed and comprehensive analyses are yet to be undertaken especially with regard to secondary sources of CO and the chemical response to changes in CO within the context of coupled chemistry-climate studies. Systematic investigation of these confounding interactions is warranted as we move forward toward producing long-term chemical reanalysis for climate studies and attribution.

1.3. Objectives of This Study

Here we investigate the first year of a reanalysis project at the National Center for Atmospheric Research (NCAR), which focuses on assimilating the multispectral MOPITT CO retrievals for more than a decade (2002 to 2015). We have initiated our reanalysis (state estimation) for the year 2002 using our previously described assimilation system [*Arellano et al*., 2007; *Barré et al*., 2015], which includes an ensemble-based DA software (Data Assimilation Research Testbed, or DART) and the coupled chemistry-climate model of

the Community Earth System Model (or CESM) *Hurrell et al.* [2013] Community Atmospheric Model with Chemistry (or CAM-Chem). Hereafter, this DA system will be denoted as DART/CAM-Chem and our most recent study [*Barré et al.*, 2015] as B2015. This reanalysis finds the best estimate of the CO atmospheric state by optimizing its concentration (i.e., state as opposed to state-source estimation). Here we tackle the two first issue mentioned earlier regarding accuracy and consistency of concentration and emission trends due to errors in model representation of physical and chemical processes. We focus in particular on assessing the impact on the chemical system when CO distribution alone is constrained in CESM.

The specific objectives of this paper are twofold.

First, we conduct a global evaluation of the impact of MOPITT assimilation on modeled CO fields by (a) investigating the full diagnostics of assimilated MOPITT observations (e.g., bias, root-mean-square error (RMSE), mean of analysis increments, and chi-square) and (b) comparing the simulated CO fields to ground-based and airborne CO measurements. These comparisons provide a comprehensive evaluation of the changes in CO distribution resulting from assimilating MOPITT. Our evaluation serves as a direct extension of B2015, with a particular focus on evaluating our system over a longer assimilation period (1 year versus one season). This evaluation is conducted within the context of chemical reanalysis rather than chemical weather application as in B2015. Furthermore, we note that such evaluation is a necessary first step to build confidence on our analysis of CO distributions.

Second, we investigate the detailed chemical response of CESM/CAM-Chem to MOPITT assimilation. In particular, we focus on the impact of CO assimilation (state estimation) on the modeled tropospheric chemistry and methane lifetime through changes in the CO burden. We study the spatiotemporal patterns of the changes in concentrations, chemical fluxes, and lifetimes of relevant species affecting the CO-OH-CH_4 and VOC/NO_x/O_3 chemical systems; i.e., what is the short-term model response in CO-OH-CH_4 and VOC/NO_x/O_3? This study collectively addresses the issues pointed out by recent reanalysis [*Inness et al.*, 2015; *Miyazaki et al.*, 2015] and inverse modeling studies [*Fortems-Cheiney et al.*, 2011; *Yin et al.*, 2015] within the context of state estimation, coupled chemistry-climate modeling, the use of the new multispectral MOPITT retrievals of CO profiles, and fully and explicitly accounting for nonlinear processes.

Together, these two aim to provide unique perspectives on the impact of constraining the CO distribution in atmospheric chemistry models. To our knowledge, this is the first systematic investigation on the chemical system in a context of global assimilation. Yet this has important and broad implications to the design approach, observing systems, implementation, and interpretation of ongoing and future chemical reanalysis, source inversion, and chemistry-climate studies. Understanding the model response provides insights on how to accurately and consistently attribute the mismatch between modeled and observed distribution of radiatively and chemically active species like O_3 and CH_4 that are significantly and nonlinearly affected by changes in CO.

The paper is organized as follows. In section 2, we describe the CESM/CAM-Chem model, the data assimilation system (DART), the MOPITT CO observations, and the data sets used for verification. In section 3, we evaluate and contrast the simulated CO fields, the assimilated observations, and the independent measurements. The impact of the assimilation on the CO concentrations, proportions of CO burden, and other chemical species are described in section 4. We discuss our results in section 5. Our summary, conclusions, and description of future prospects are presented in section 6.

2. Chemical Data Assimilation System

This section presents the following main components of our chemical data assimilation system: (1) main observations to be assimilated (MOPITT CO retrievals), (2) chemical transport model (CESM/CAM-Chem), and (3) data assimilation (DA) software (DART) integrating MOPITT measurements into CAM-Chem. Although this DA system has been described in detail by B2015 and references therein, we will briefly describe the system once again to provide context with other reanalysis/inverse analysis studies, specifically *Inness et al.* [2015], *Miyazaki et al.* [2015], and *Yin et al.* [2015]. We also briefly describe the CO tags which were not included in B2015. We use these tags as tracer diagnostics. In this section, we also describe our experimental design for the reanalysis. We note that this system assimilates both meteorological observations from the National Centers for Environmental Prediction (NCEP) and MOPITT CO retrievals and can allow updating

both meteorological and chemical states. Finally, we describe the observations used for the evaluation of the simulations.

2.1. MOPITT Retrievals

The MOPITT instrument is a nadir-viewing, cross-track scanning gas correlation radiometer on board the NASA EOS Terra satellite. It operates in both the thermal (4.7 μm) and near (2.7 μm) infrared [*Edwards et al*., 1999]. The V5J data set used in this study is the product of a multispectral retrieval algorithm [*Worden et al*., 2010] that provides total CO column as well as CO profiles expressed in 10 levels (10 partial CO columns), nominally located from the surface to 100 hPa. Multispectral retrievals show, in general, increased sensitivity to CO with respect to thermal infrared-only retrievals, in particular for daytime measurements over land. Overall, the Degree of Freedom for Signal (DFS), which is a metric of instrument sensitivity, is generally close to 2 and greater than 1 [*Worden et al*., 2010]. Validation of V5J retrievals shows bias values below 5% in the lower troposphere (surface to 400 hPa) and around 14% in for the upper troposphere [*Deeter et al*., 2013]. To avoid introducing a positive bias in their analyses, *Jiang et al*. [2013] and B2015 excluded MOPITT retrievals from the upper three levels (300, 200, and 100 hPa). Similarly, we only assimilate retrievals from the lower seven levels (i.e., surface to 400 hPa). Regarding assimilation purposes, model profiles are "smoothed" using the MOPITT a priori profiles and averaging kernels to match the vertical resolution of the retrievals. However, we assign to each partial column the pressure level where its averaging kernel peaks, so as to be consistent with its associated retrieval sensitivity. For each partial column, we use an error variance corresponding to the diagonal element of its retrieval error covariance matrix. We assume that the off-diagonal error terms are relatively small, to sequentially assimilate each partial column of the profile. For purposes of quality control related to cloud detection and measurement sensitivity, we use only daytime data, with DFS greater than 0.5, within 65° latitude of the equator. To minimize introduction of noise in the model due to subgrid variability and horizontal error correlation in the data, we use the error-weighted average of the data within the model grid (i.e., superobservations), assuming uncorrelated errors of pixels within it. We choose to assimilate the full lower seven levels of the profile to extract as much information as there is in MOPITT (e.g., retrievals with DFS >1) for our purpose of constraining the full 3-D CO distribution.

2.2. Community Earth System Model, CESM

In this study, we use the version 1.2 of the NCAR Community Earth System Model (CESM), with updates as described in *Tilmes et al*. [2015], available for download at http://www.cesm.ucar.edu/experiments/cesm1.2/. It consists of different component models of the climate system, mainly the Community Atmosphere Model, Version 4 (CAM4) [*Neale et al*., 2013], the Community Land Model Version 4.0 (CLM4) [*Lawrence et al*., 2011], the Parallel Ocean Program (POP2) [*Smith et al*., 2010], and the Community Ice Code (CICE4) [*Hunke and Lipscomb*, 2008]. Here we prescribe sea surface temperatures and sea ice for present-day conditions [*Rayner et al*., 2006] and include only the coupling between land and atmosphere. Model dynamics are calculated online but are constrained by observations due to the assimilation of conventional meteorological data sets (see section 2.3). We focus here on the simulation of CO in the Community Atmosphere Model with Chemistry (CAM-Chem) as described and evaluated in *Lamarque et al*. [2012] and *Tilmes et al*. [2015]. We use an active coupling with CLM4 [*Lawrence et al*., 2011] to allow online calculation of the dry deposition of gases and aerosols [*Val Martin et al*., 2014] as well as biogenic emissions through the Model of Emissions of Gases and Aerosols from Nature (MEGAN) version 2.1 in CLM [*Guenther et al*., 2012]. The leaf area index is prescribed using Moderate Resolution Imaging Spectroradiometer (MODIS) products. Model dynamics are calculated using the CAM4 finite volume (FV) dynamical core [*Neale et al*., 2013], which includes horizontal and vertical transport of the chemical tracers. The spatial grid spacing is 1.9° in latitude and 2.5° in longitude, with 26 vertical levels with a model top at around 40 km. The chemical composition of O_3, NO, NO_2, HNO_3, CO, CH_4, N_2O, and N_2O_5 in the top five vertical levels of the model (stratosphere) are prescribed using values from previous simulations of the Whole Atmosphere Community Climate Model (WACCM) [*Marsh et al*., 2013] for present-day conditions (monthly averages from 1996 to 2005). No stratospheric reactions are considered in this study. In the troposphere, we used full chemistry mechanism from MOZART v4 [*Emmons et al*., 2010] which has been updated and summarized in *Lamarque et al*. [2012] and *Tilmes et al*. [2015]. The bulk aerosol model (BAM) is used to represent aerosol mass at specific diameters and species. Global monthly anthropogenic emissions are based on the RCP8.5 inventory [*Granier et al*., 2011]. This inventory is the basis for the MACCity inventory [*Granier et al*., 2011] and is consistent with the

historical inventory used for the CCMI activity [*Lamarque et al*., 2010]. Total anthropogenic CO emissions for year 2000 (~610 Tg CO/yr) are higher in this inventory relative to EDGAR (~550 Tg CO/yr) [see *Granier et al*., 2011, Figure 1]. We use this inventory since it provides a longer time series with information on interannual trends covering the period of this reanalysis. Daily fire emission estimates have been precalculated using the Fire Inventory from NCAR (FINN) version 1.5 [*Wiedinmyer et al*., 2011] and have been averaged on a monthly basis. The study by *Wiedinmyer et al*. [2011] provides a comparison with GFED3.1 and FINNv1, showing the ratio of FINN to GFED emissions to be slightly higher in CO (1.07 to 1.38) and much higher in VOCs (3.8 to 5.0), for example. Emission fields for total CO for each season are shown in the supporting information. We refer the reader to these studies for details on the anthropogenic and fire emission inventories. We note here that previous studies have used either a simplified chemistry or full chemistry scheme in an offline chemistry transport model or CTM [*Yin et al*., 2015; *Miyazaki et al*., 2015] or a full chemistry in a weakly coupled chemistry-weather model [*Inness et al*., 2015]. While our system includes full chemistry in a fully coupled model, this study only utilizes coupling between meteorology, land, and atmospheric chemistry. This serves as an online CTM, which enables us to focus on investigating the atmospheric chemistry component of CESM.

2.3. Data Assimilation Research Testbed

The Data Assimilation Research Testbed (DART) is an open source community software facility (http://www.image.ucar.edu/DAReS/) for ensemble data assimilation [*Anderson et al*., 2009a]. DART works with a wide variety of numerical models and observations, and its modularity provides a flexible environment for data assimilation research, development, and education. The CESM/CAM-Chem modeling system interfaces with DART and allows sequential assimilation of both meteorological and chemical observation using the Ensemble Adjustment Kalman Filter (EAKF) scheme [*Anderson*, 2001]. A similar ensemble square root filter algorithm (Local Ensemble Kalman Filter or LETKF) was used by *Miyazaki et al*. [2015] for assimilating chemical measurements in a CTM. For this application, the EAKF algorithm begins with an ensemble of CESM forecasts defined as one multi-instance CESM run (see section 2.3.1) and followed by an analysis step that updates the atmospheric states in light of available observations (see section 2.3.2).

2.3.1. Ensemble Forecasts

We use a 30-member ensemble of 6 h coupled (meteorology/land/chemistry) forecasts with the active coupled model components CAM-Chem and CLM as the prior for the our analysis. During each forecast, the CESM coupler exchanges fluxes at every 30 min solver time step. The ensemble forecast of meteorology provides a spread in chemistry through perturbations in the initial condition of meteorological state variables such as horizontal winds, boundary layer dynamics, temperature, and specific humidity. Those perturbations not only affect the transport of CO but also directly influence the spatial distribution of chemical species, through ensuing perturbations in deposition rates, photolysis, heterogeneous chemistry (with moisture), as well as in land surface conditions (biospheric/oceanic/land fluxes). The benefit of using an ensemble of model simulations initialized by an EnKF has been demonstrated in the context of CO_2 assimilation [*Liu et al*., 2011]. We also add perturbations in emissions to incorporate associated uncertainties in emissions to the spread (errors) in tropospheric concentrations of chemical species. Those perturbations are carried out using pseudorandom and normally distributed realizations following *Evensen* [2003], as applied in *Gaubert et al*. [2014]. Here we use a horizontal length scale of 1000 km and standard deviation of 40% for CO and 30% for VOCs. These values are chosen based on previous DA setup and comparison of emission inventories [B2015; *Granier et al*., 2011]. The aim is to represent a realistic spread from errors in emissions. The same "noise" is applied to all CO sources and VOCs across all time steps. We note that using additive relative perturbations does not change the a priori spatial and temporal distributions as well as cross covariances between chemical variables for the ensemble mean. We also perturbed surface CH_4 (which is prescribed in CAM-Chem) by adding a global constant value for each ensemble member. The spread in CH_4 has been set to lower values (10%), because it is prescribed from an observational data set.

2.3.2. Analysis Procedure

As mentioned, we use the Ensemble Adjustment Kalman Filter (EAKF) scheme by *Anderson* [2001] for our analysis. This is an ensemble Kalman filter with a deterministic update that ensures that the posterior ensemble mean and covariance are consistent with Kalman filter theory. Ensemble Kalman filters have been successfully applied in tropospheric chemistry for surface observations [*Hanea et al*., 2004; *Constantinescu et al*., 2007a, 2007b; *Wu et al*., 2008; *Zubrow et al*., 2008; *Tang et al*., 2011; *Curier et al*., 2012; *Gaubert et al*., 2014] and satellite retrievals [*Arellano et al*., 2007; *Miyazaki et al*., 2012b; *Coman et al*., 2012; B2015]. The best performance is

achieved by correcting the raw sample error covariances via inflation and localization to minimize filter divergence and sampling error. Here we briefly describe the EAKF algorithm as implemented in DART. We refer the reader to *Anderson et al*. [2009a, and references therein] for more a detailed description of the algorithm. For this study, we use the DART/EAKF system that has been coupled with CAM [*Raeder et al*., 2012] for meteorological DA and with CAM-Chem [*Arellano et al*., 2007; B2015] for MOPITT CO retrieval DA. As with previous studies, the NCEP/NCAR conventional meteorological observations of pressure, air temperature, winds, and specific humidity are assimilated. This includes surface observations (land and marine), radiosondes, the Aircraft Communications and Reporting System (ACARS), and satellite drift winds. Data processing, model configurations, and assimilation setup in the case of meteorological DA have been taken from the atmospheric reanalysis by *Raeder et al*. [2012].

The DART/EAKF procedure, which is based on sequential DA, is as follows:

1. Generate an ensemble of CAM-Chem 6-hourly forecasts (section 2.3.1).
2. Apply a space and time adaptive inflation factor to adjust the prior error variance as described in *Anderson* [2009b]. Here the ensemble is linearly inflated around its mean by increasing the deviation of each ensemble member by a factor larger than 1. This factor is sequentially optimized in space by correcting the spread according to the innovation and the associated total error. Generally, the inflation factor values are larger in densely observed regions, where the posterior spread is usually too low.
3. Apply associated forward operator to get an ensemble of expected observations. For each ensemble member, we transform the corresponding model profile of CO at the observation location to a partial column y^{CAM} that is the model equivalent of MOPITT CO partial column. Given the a priori profile $y_{\mathrm{apr}}^{\mathrm{SAT}}$ and its averaging kernel matrix $\boldsymbol{A}$, the smoothed CAM-Chem profile that is directly comparable to MOPITT observations is calculated by

$$y_{\mathrm{ret}}^{\mathrm{CAM}} = 10^{\boldsymbol{A}\log_{10} y^{\mathrm{CAM}} + (\boldsymbol{I}-\boldsymbol{A})\log_{10} y_{\mathrm{apr}}^{\mathrm{SAT}}} \tag{1}$$

4. Update the prior ensemble member j in observation space ($y_{m,j}^{f}$) using the observation y_o, its error σ_o, the ensemble mean $\overline{y}_m^f$, and standard deviation σ_m^f. The posterior ensemble is expressed as

$$y_{m,j}^{a} = \left[\sqrt{\frac{(\sigma_o)^2}{(\sigma_o)^2 + (\sigma_m^f)^2}}\right]\left[y_{m,j}^{f} - \overline{y}_m^f\right] + \left[\frac{\overline{y}_m^f}{(\sigma_m^f)^2} + \frac{y_o}{(\sigma_o)^2}\right]\left[\frac{1}{(\sigma_m^f)^2} + \frac{1}{(\sigma_o)^2}\right] \tag{2}$$

The corresponding increment in observation space for ensemble member j is the difference between the posterior and prior:

$$\Delta y_{m,j} = y_{m,j}^{a} - y_{m,j}^{f} \tag{3}$$

Update the prior ensemble in model space by first calculating linear regression coefficients (sensitivity) between the ensemble of a prior state and expected observations. This least squares approach is described in detail by *Anderson* [2003]. We can then multiply these coefficients by the increment in observation space $\Delta y_{m,j}$ to estimate the analysis increment in model space for ensemble member j. That is,

$$\Delta x_j = \alpha \frac{\sigma\left(x^f, y_m^f\right)}{\left(\sigma_m^f\right)^2} \Delta y_{m,j} \tag{4}$$

where Δx_j is the increment in model space, $\sigma\left(x^f, y_m^f\right)$ is the covariance between the observation and the model state, and α is a localization function applied for error covariance localization (or tapering). This error covariance localization is done to avoid spurious long-range correlation due to finite ensemble size. We use the Gaspari-Cohn (GC) fifth-order rational function [*Gaspari and Cohn*, 1999] with compact support to taper the covariance of the state farther away from the observation location. This tapering is defined by a half-width parameter, which is the distance at which the value of α is 0.5. As in *Raeder et al*. [2012], we used a half width of 0.2 rad in the horizontal (~1200 km) and 200 hPa in the vertical. This is larger than the localization range in B2015. Differences in half widths, however, do not significantly affect the analysis results (B2015).

Although the current DART/EAKF setup is capable of updating all CESM model states in the state vector for any observations, we opted to use here a variable localization as defined in *Kang et al*. [2011]. In particular, we use univariate assimilation for CO, meaning that only the CO observations are impacting the CO concentrations. We opted to do this for two reasons. First, we suppose that since we are using the same setup as *Raeder et al*. [2012], the current sets of meteorological data that we used here already provide reasonable constraints on meteorological state variables such as winds, temperature, surface pressure, specific humidity, cloud liquid content, and cloud ice content. Second, we have low confidence at this stage in the cross correlation generated by the ensemble and in the model short-term feedback of chemical perturbations to meteorology. Inference of chemical parameters from meteorological data assimilation can lead to unphysical values in the chemical state of the atmosphere. This is a subject we would like to pursue in future studies.

2.3.3. CO Tags

Several emission sources have been "tagged" in order to reconstruct the composition of the modeled CO. As in *Emmons et al*. [2010], the additional tracers are treated in the same manner as the total CO (e.g., the same CO + OH loss mechanism but without affecting OH). The tags correspond to the global direct CO emissions from the main sectors such as anthropogenic, biomass burning, biogenic, and oceanic sources, the sum of these accounts for the primary component of the total CO. CO from chemical oxidation, which defines the secondary component of the total CO, can be deduced by subtracting the primary CO from the total CO. We also tagged CO derived from CH_4 using a yield of 0.9 (i.e., molar ratio of CO formed per CH_4 consumed). We note that we did not perturb emissions for these tags. The resulting ensemble spread in the abundance of these tags is due solely to the perturbations in meteorology and chemistry. These tags represent the time-varying derivatives, d[CO]/demis, or the associated response functions (in concentrations) for each emission category. The same response functions are used in Bayesian synthesis (analytical) inversions [e.g., *Arellano et al*., 2004; *Kopacz et al*., 2009] to optimize CO emissions. In our setup, however, each tag uses the full OH field calculated from the full chemistry (rather than prescribed), hence accounting for nonlinear effects of changes in OH due to changes in total CO. Furthermore, in the case of the MOPITT assimilation, we update these response functions (i.e., tagged CO concentration fields) rather than optimizing the emissions. At every 6-hourly assimilation, each CO tag ($CO^f_{i,j}$) for ensemble member j is scaled after the analysis step (equation (4)) of the assimilation cycle according to its relative a priori response contribution to the total CO forecast concentration (CO^f_j), i.e.,

$$CO^a_{i,j} = CO^f_{i,j} + \frac{CO^f_{i,j}}{CO^f_j}\Delta CO_j \tag{5}$$

where ΔCO_j is the CO analysis increment in model space (Δx_j in equation (4)). This ensures that the sum of CO tags is equal the total CO constrained by MOPITT. In doing this, we update the response functions rather than the emissions. Again, we note that the emissions in the forecast model CAM-Chem are not updated during the update step of assimilation. The CO tags, which do not feed back to the model chemical system, are used for tracer diagnostics to help understand the changes in CO burden due to CO state assimilation. The updated CO tags represent therefore the MOPITT-constrained CO burden due to every emission category.

2.4. Experimental Setup and Initialization

We assess the impact of MOPITT assimilation over 1 year by carrying out two assimilation experiments: (1) Control Run, where only 6-hourly meteorological observations are assimilated, and (2) MOPITT Reanalysis, where MOPITT V5J CO profiles are jointly assimilated with meteorological observations. The initialization was carried out in two steps. First, we performed two deterministic ("single-model") 1 year CAM-Chem runs starting 1 January 2001. The first run was then used to spin-up the model with the new variables (CO tags). Next, the fields from 1 January 2002 were used as initial condition for the second run in 2001. In the second step, we run an ensemble simulation (started with small perturbations on the temperature initial conditions) from the deterministic run on 1 November 2001. This ensemble simulation also includes (a) perturbations in CH_4 and emissions as described in section 2.3.1, (b) 6-hourly meteorological DA, and (c) 6-hourly MOPITT CO DA (starting 30 November 2001). As previously described, perturbations in deposition and biogenic emissions result from perturbations in meteorology. We chose to start CO DA only after 1 month of meteorological DA. Finally, on 30 January 2002, the Control Run is initialized from the MOPITT Reanalysis. The Control Run and the MOPITT Reanalysis have exactly the same setup, using the same initial conditions. This means that

Table 1. List of Measurements Used for Model Evaluation[a]

	Measurement Data Sets	Sites/Domain	References
Network	**MOZAIC/IAGOS**	Europe	*Marenco et al.* [1998]
Measurement type	Aircraft in situ Measurements	U.S. and Canada	*Nédélec et al.* [2003]
Spatial average	Continental/100 hPa bin		
Temporal average	Seasonal		
Campaign	**SMOCC**	Amazon	*Andreae et al.* [2004]
Measurement type	Aircraft in situ measurements		
Spatial average	29 flights/500 m bin		
Temporal average	2 months		
Network	**WMO/WDCGG**	Global	*Novelli and Masarie* [2015]
Measurement type	Surface measurements		
Spatial average	None		
Temporal average	Annual		
Network	**NDACC** (www.ndacc.org)	Ny Alesund	*Notholt et al.* [1993]
Measurement type	Ground-based solar absorption	Thule	*Hannigan et al.* [2009]
	Fourier Transform Infrared Spectrometer	Toronto	*Whaley et al.* [2015]
Spatial average	Profile mixing ratio values at altitudes	Wollongong	*Paton-Walsh et al.* [2005]
	higher than 5 hPa taken from the a priori	Lauder	*Morgenstern et al.* [2012]
Temporal average	Available at spectra retrieval times,	Arrival Heights	*Zeng et al.* [2012]
	compared as month averages		

[a]The location of the measurements is indicated in Figure 1.

there are 2 months (from 30 January 2002 to 1 April 2002) for which the influence of MOPITT assimilation can be seen in the Control Run. In order to remove the effect of optimized initial conditions from prior MOPITT assimilation, we focus on the period from 1 April 2002 to 1 April 2003 for our evaluation and chemical fluxes calculations.

2.5. Observational Data Sets Used for Evaluation

We use multiple independent data sets of CO that are available to evaluate the forecast and analysis of our control and reanalysis runs. These data sets are measurements of CO taken from different observing platforms (aircraft and ground, during routine observations, or field campaigns) and with various sampling/instrument characteristics (infrared analyzer, spectrometer, and flasks). The combination of these measurements provides a comprehensive evaluation of the four-dimensional CO fields (e.g., ground sites at remote locations; aircraft profiles over North America, Europe, and the Amazon; and column retrievals from ground sites at high latitudes). Some characteristics of the observations are shown in Table 1, while their geographical distribution can be seen in Figure 1.

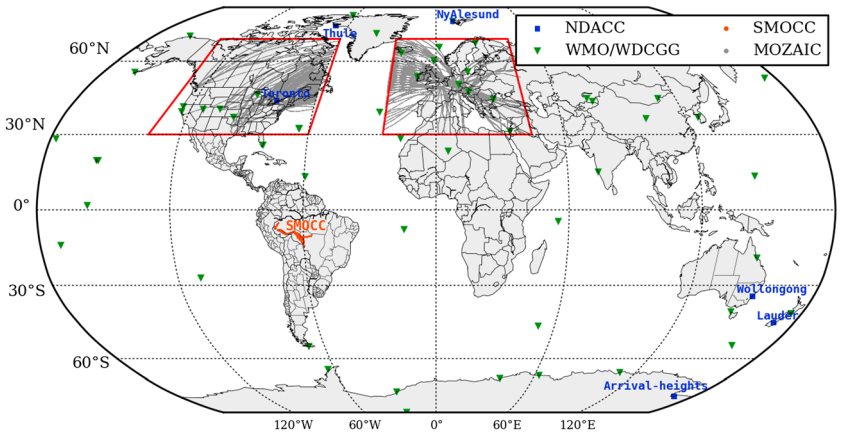

Figure 1. Locations of measurements used in our model evaluation. Grey lines show all MOZAIC aircraft observations within the specified domain (outlined here in red). Orange lines show all SMOCC aircraft observations. Blue squares indicate the location of column measurements taken at NDACC stations, and green triangles show the location of surface in situ measurements at WDCGG stations.

2.5.1. WDCGG Measurements

We use CO measurements from the World Data Centre for Greenhouse Gases (WDCGG) database (http://ds.data.jma.go.jp/gmd/wdcgg/). Most of those measurements come from the NOAA Global Monitoring Division (NOAA/GMD) surface sites [*Novelli and Masarie*, 2015]. These high-precision measurements, which are taken at remote sites (mountains and oceanic islands), are representative of large-scale background CO at the surface. Measurements have been obtained from 56 individual stations for this period (Figure 1).

2.5.2. NDACC-FTS Measurements

We use CO total column retrievals acquired with ground-based high-resolution solar absorption Fourier transform spectrometer (FTS) at six Network for the Detection of Atmospheric Composition Change (NDACC) stations (http://www.ndsc.ncep.noaa.gov/). First, simulated vertical profiles have been interpolated and smoothed by the associated observational a priori profile and averaging kernel for each retrieval over the time period March 2002 to April 2003. Then, measured and modeled total columns are monthly averaged prior to comparison. We use three sites located in the Northern Hemisphere (NH): one at midlatitudes, Toronto in Canada [*Whaley et al*., 2015; *Wiacek et al*., 2007], and two at high latitudes, Thule in Greenland [*Hannigan et al*., 2009] and Ny Alesund in Spitsbergen [*Notholt et al*., 1993, 1997]. We also use three sites located in the Southern Hemisphere (SH): Wollongong, in Australia [*Paton-Walsh et al*., 2005] and Lauder in New Zealand [*Morgenstern et al*., 2012] as well as Arrival Heights in Antarctica [*Zeng et al*., 2012]. The location of the sites can be found in Figure 1.

2.5.3. MOZAIC-IAGOS Measurements

The MOZAIC database (Measurement of Ozone and Water Vapor by Airbus In-Service Aircraft) [*Marenco et al*., 1998], a part of the IAGOS consortium (In-Service Aircraft for a Global Observing System), contains 20 years (1994 to 2015) of in situ ozone, CO, and total nitrogen (NO_y) measurements, acquired from commercial aircrafts. CO is measured using an infrared analyzer with ±5% with an absolute error minimum of 5 ppb [*Nédélec et al*., 2003]. Most measurements are performed at cruising altitude (i.e., in the upper troposphere); quasi-vertical profiles are obtained during takeoff and landing. We produced seasonally averaged vertical profiles for two densely sampled regions (Figure 1), North America and Europe [*Thouret et al*., 2006]. CO measurements for all the flights in each of these two regions were segregated in 100 hPa bins and averaged to obtain a mean vertical profile. There are thousands of observations below 350 hPa and around 12,000 above 350 hPa (Figure S1 in the supporting information). The former, mostly situated over the Atlantic Ocean, are representative of the upper troposphere and the latter of the continental lower troposphere. Measurements closest to the surface sample airports and their surroundings. Therefore, they may represent highly polluted air from local sources.

2.5.4. Aircraft Observations From the LBA-SMOCC Campaign

A suite of 29 flights (Figure 1) over the Amazon forest during the Large-Scale Biosphere Atmosphere Experiment in Amazonia-Smoke, Aerosols, Rainfall, and Climate (LBA-SMOCC) field campaigns have been used to complement this evaluation [*Andreae et al*., 2004]. These in situ CO profiles were taken from aircraft observations during the end of the dry season (September and October 2002) [see *Fuzzi et al*., 2007, Figure 2] over the Amazon basin in Brazil, affected by plumes from strong vegetation fires. Measurement details have been described in *Guyon et al*. [2005]. Some of these measurements were close to strong local fires, sometimes leading to pyroconvections, which are processes occurring at model subgrid scales [*Freitas et al*., 2006, 2007]. The observed CO concentrations in the lower 1000 m are driven by tens of thousands of fires across the entire perimeter of the Amazon forest [*Guyon et al*., 2005; *Andreae et al*., 2012]. Aircraft passages through the plumes of nearby fires resulted in CO concentration peaks up to 5000 ppb. In order to remove the strong local effects that would bias the evaluation, CO concentrations greater than 450 ppb were removed. For the purpose of evaluation, all flights were averaged and binned in 500 m bins. The number of observations and a zoomed map of observations are shown in Figures S2 and S3 in the supporting information.

3. Verification of Assimilation Results

This section describes the diagnostics and comparisons with assimilated and independent data that are used to evaluate the assimilation results.

3.1. Observation Space Diagnostics

Here we show the diagnostics derived from comparing assimilation results with meteorological and MOPITT data that were assimilated.

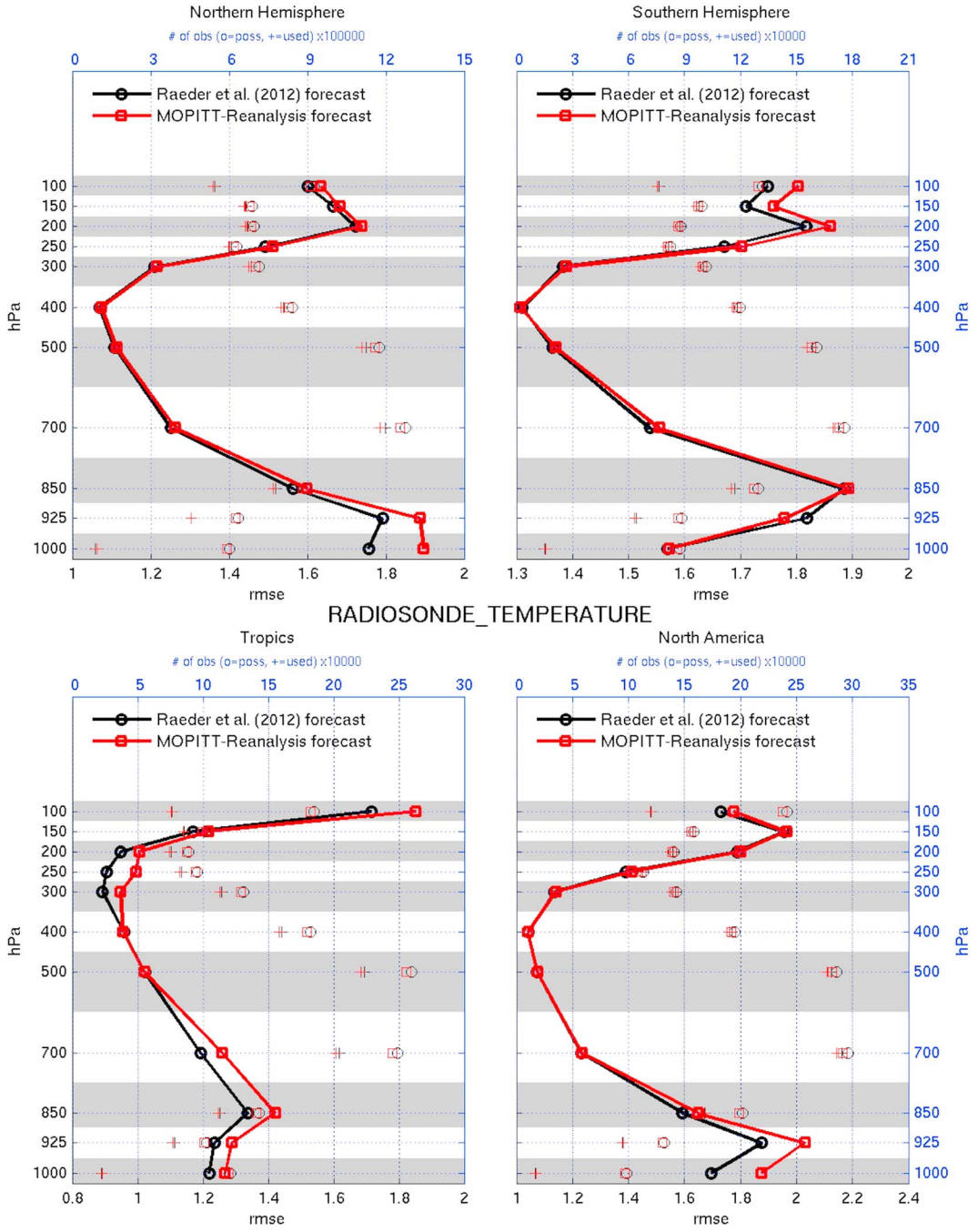

Figure 2. Average annual vertical profile of RMSE against temperature measurements (in K) by radiosondes over (top left) the Northern Hemisphere, (top right) the Southern Hemisphere, (bottom left) the tropics, and (bottom right) over North America. The black points show the results for the mean of the ensemble of 6 h forecast from *Raeder et al.* [2012], while the red points show the equivalent for the MOPITT Reanalysis run. The associated total spread and bias are presented in the supporting information. We note here that previous reanalysis (except *Inness et al.* [2015]) used prescribed meteorology to drive the CTM which may introduce numerical inconsistencies and does not allow internal feedback within the assimilation cycle.

3.1.1. Verification of the Meteorological Assimilation

The evaluation of the meteorological assimilation will be treated only briefly in this section. Regarding this aspect, most of the model and assimilation parameters were taken from *Raeder et al.* [2012]. The main difference is the use of only 30 ensemble members here instead of 80 ensemble members in *Raeder et al.* [2012]. The spatial localization length may be too broad in our case. We compare the performances of the two

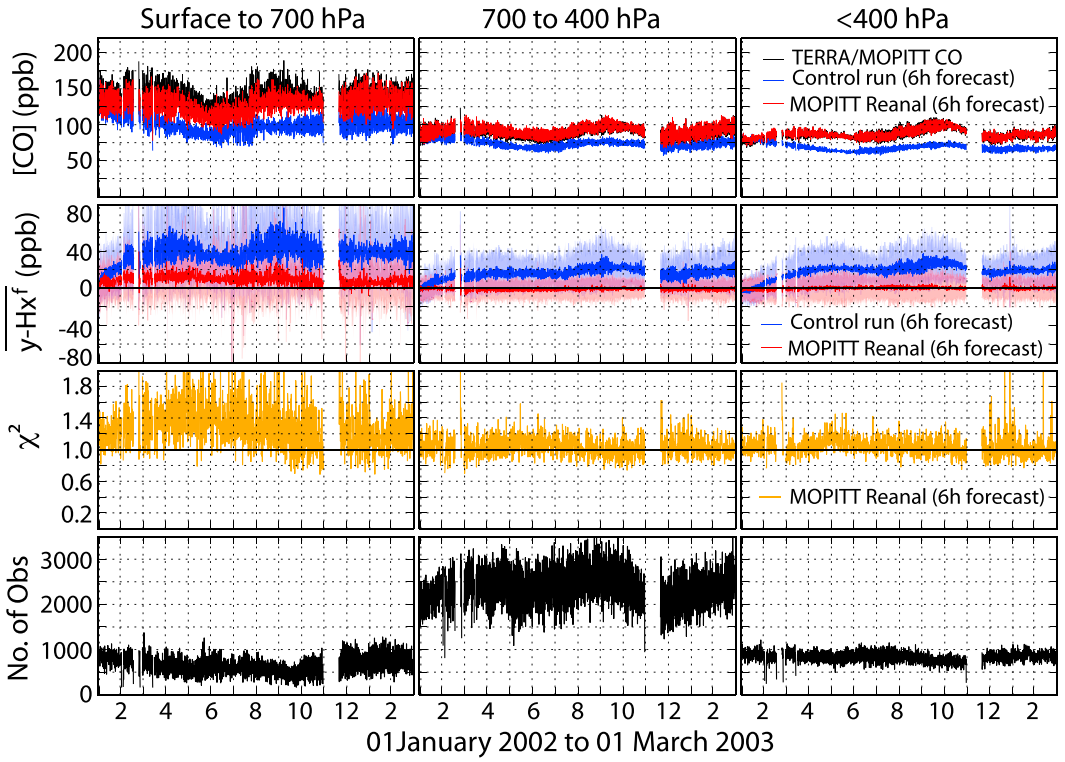

Figure 3. Time series of global assimilation diagnostics in observation space. For every assimilation step, the observations (and statistics) are averaged across the globe (horizontal) and over vertical sections: (left column) lower troposphere (from surface to 700 hPa), (middle column) middle troposphere (from 700 to 400 hPa), and (right column) upper troposphere (lower pressure than 400 hPa). (first row) The CO concentrations in ppb for MOPITT in black, 6-hourly forecast from the Control Run in blue and from MOPITT Reanalysis run in red. (second row) The innovations for both runs. (third row) The chi-square statistics of the forecasts from the MOPITT Reanalysis run. (fourth row) The number of observations (number of observation per 6 h) successfully assimilated in CAM-Chem and for which statistics are calculated.

reanalyses by comparing the root-mean-square error (RMSE) of 6 h forecasts of temperature against radiosondes (Figure 2). The forecast performance is similar between experiments with an expected but only slight degradation in MOPITT Reanalysis relative to *Raeder et al*. [2012] due to our use of smaller ensemble size. However, the MOPITT Reanalysis exhibits a RMSE in temperature lower than 2 K while the mean bias is lower than 1 K, which is within the errors in observations. Moreover, the total spread mimics the RMSE shape and amplitude, indicating a good estimation of errors by the ensemble (see Figures S4 and S5 in the supporting information).

3.1.2. Verification of the MOPITT CO Assimilation

The statistics for each assimilation step across the entire year of the analysis period is shown in Figure 3. This is calculated using observations that were successfully assimilated in CAM-Chem. The number of observations is plotted in Figure 3 (fourth row). Note that there are differences in the numbers of assimilated observations between lower, middle, and upper troposphere. These differences are due to the fact that the vertical position center of the GC localization function corresponds to the location of the maximum in the averaging kernel (see section 2.1). On average, less than 20% of all observations are assigned to pressures higher than 700 hPa (closer to the surface); another 20% are assigned to pressures lower than 400 hPa (upper troposphere). The low numbers in the upper troposphere also reflect the exclusion of MOPITT retrievals from pressure levels less than 300 hPa. The remaining 60% of all observations are assigned to the middle troposphere where MOPITT retrievals sensitivity peak (maximum values of the averaging kernel functions). The number of observations assimilated is higher during summer than winter at midlatitude and high latitudes; the tropics show no seasonal differences (not shown). The time series of global average CO loading in the lower troposphere shows two peaks (CO at about 160 ppb) in late NH Spring (April and May) and September and a minimum in NH summer (CO at about 120 ppb in July). This is indicative of the interplay between production (emissions) and loss of CO including strong seasonality of vegetation fires. The seasonal variability of CO in

the Control Run is not as pronounced as in the MOPITT data or in the MOPITT Reanalysis, although the timing of the minimum is similar. This discrepancy is clearly shown in the Control Run mean CO bias, which is about 60 ppb in early May and late September. CO from the reanalysis shows similar seasonality but with lower and systematically negative bias relative to MOPITT of about 10 ppb. This bias may be attributed to a combination of (a) possible underestimation of average surface emissions, (b) higher OH in CAM-Chem, and (c) possible systematic bias in MOPITT. An efficient diagnostic of the error specifications and their balance with actual model-observation mismatch is to use the chi-square statistics [*Ménard and Chang*, 2000]. In DART, the diagnostic is averaged across p observations at a given time step knowing the innovations for each ith observation $\left(y_o - \overline{y}^f_m\right)$ weighted by its associated errors in the forecast ($\sigma^f_{m,i}$) and observation ($\sigma_{o,i}$). This diagnostic is defined as

$$\overline{\chi^2} = \frac{1}{P}\sum_{i=1}^{P}\left(y_{o,i} - \overline{y}^f_{m,i}\right)^2 \Bigg/ \left(\left(\sigma^f_{m,i}\right)^2 + \left(\sigma_{o,i}\right)^2\right) \tag{6}$$

A value greater than 1 indicates an underestimation of the actual model and observation mismatch, while a value less than 1 suggests an overfitting of the observations. For the lower levels and mostly during spring and summer, the chi-square statistics are around 1.2 and 1.6, meaning that the MOPITT Reanalysis is persistently underestimating the total spread (observation errors and/or ensemble spread) and/or underestimating CO (bias). Note that in our calculation the forecast ensemble spread $\sigma^f_{m,i}$ has already been inflated prior to analysis update (step 2 in section 2.3.2). Inflation factors at the model surface level range from 1.2 to 1.7 in relatively denser data regions close to the sources where analysis spread is typically low. This gives us insights on the nature of our errors. We find that lower total spread can be addressed by increasing the model noise due to emissions and/or MOPITT error (which is assumed to be uncorrelated). However, it is likely that the CO bias is due to the errors in surface boundary conditions, in general, and that emission or surface fluxes in particular are causing this underestimation. While adaptive inflation plays a role in achieving a chi-square of about 1, it is dependent on data density and information content (i.e., data driving the reduction in analysis spread). This is clearly represented in the forecast statistics resulting from the assimilation of middle and upper tropospheric levels, where most of MOPITT retrievals are sensitive. Statistics are nearly perfect over the entire year. The average bias is zero, and the bias standard deviation is around the observation error (10 ppb or 10%). The chi-square statistics are oscillating around one across the entire reanalysis period, indicating well-balanced errors. The Control Run indicates difficulties in representing higher CO values transported to the upper troposphere in November 2002.

Figure 4 shows the time series of longitudinal average CO from MOPITT observations, Control Run, and MOPITT Reanalysis for the lower, middle, and upper troposphere. The time average statistics (bias and RMSE) are also presented in order to show the latitudinal trends in CO (Figure 4, fourth row). For fixed latitude, we see the CO seasonal cycle from MOPITT as changes in concentration (colors) across time (x axis). In the NH, the CO values are higher in winter and early spring and lower in summer, mainly in response to the OH cycle governing the CO sink. There is an associated seasonality in the interhemisphere gradient of CO (moving northward during the summer). The Control Run underestimates the winter/spring enhancement. This can be seen in its bias relative to MOPITT, close to 40 ppb for the annual average (Figure 4, third and fourth rows). The maximum latitudinal extent of this bias occurs in February, especially closer to the surface, whereas the bias minimum occurs in July. There is also a clear signal of CO enhancement from BB sources in the tropics from May to October 2002, with a maximum vertical and latitudinal extent occurring in October.

This leads to an increase in the bias in the Control Run of up to 40 ppb in October around 20° south. In contrast, the bias in the MOPITT Reanalysis is close to zero, lower than 10 ppb on average. MOPITT assimilation leads to an increase of CO across the troposphere. This changes the sign of the bias for the upper levels as compared to the Control Run. This indicates that vertical mixing of higher CO coming from the lower troposphere is too strong. However, the remaining bias in the upper troposphere is rather low compared to the Control Run bias. A band of larger CO overestimation can be seen in the tropics for both the Control Run and the MOPITT Reanalysis, indicating that model convection is perhaps slightly too strong. As expected, there is a significant improvement in the MOPITT Reanalysis. However, there are some latitudinal differences in the bias, RMSE, and bias standard deviation indicating a better fit in the midlatitudes than in the tropics.

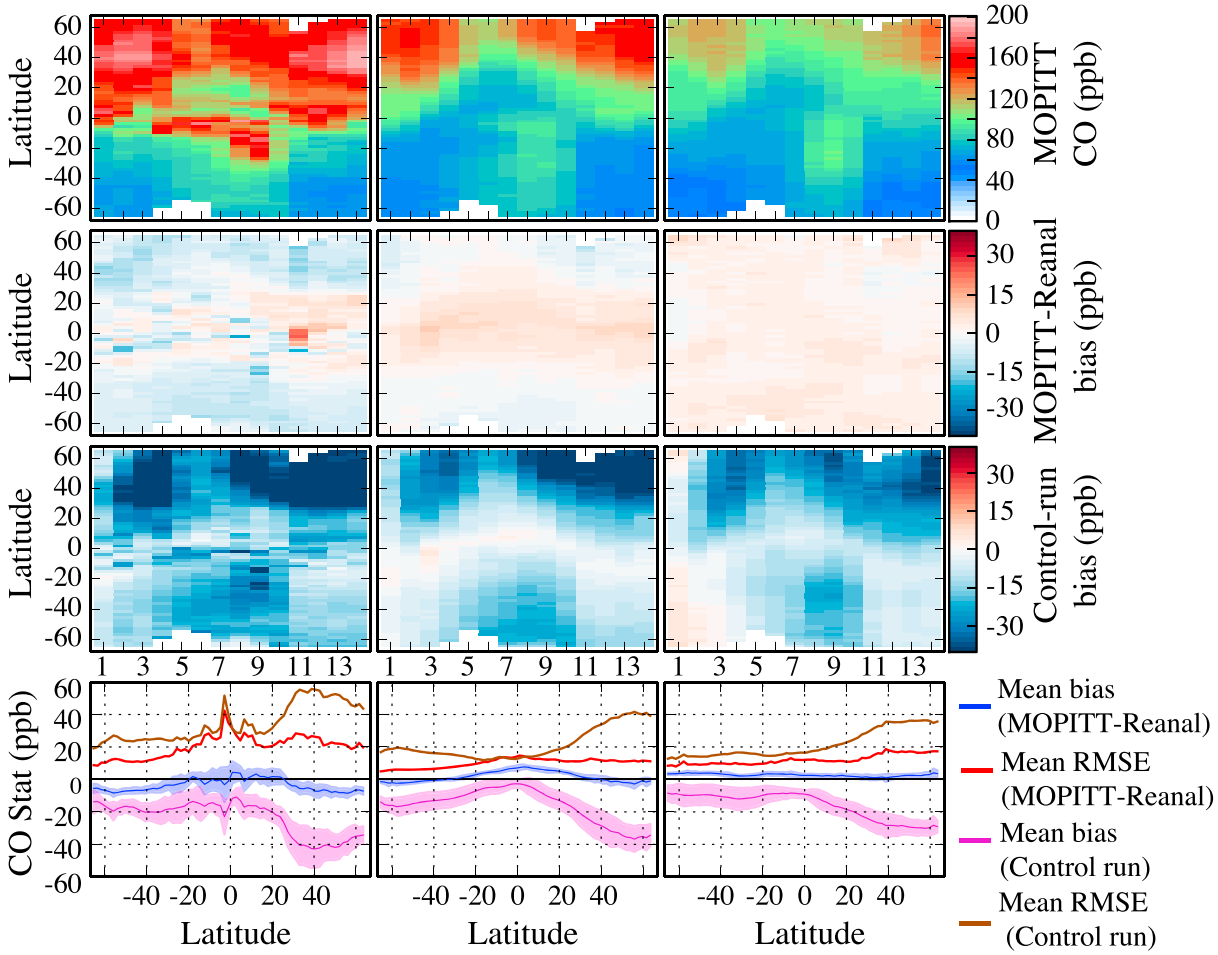

Figure 4. Monthly average latitudinal cross section of MOPITT CO in observation space for the (left column) lower troposphere, (middle column) middle troposphere, and (right column) upper troposphere. The average bias between simulations and MOPITT CO is shown for (second row) the MOPITT Reanalysis and (third row) the Control Run. The labels in the time (horizontal) axis for these plots correspond to the month in which these fields are averaged (February 2002 to March 2003). (bottom row) The time average (April 2002 to April 2003).

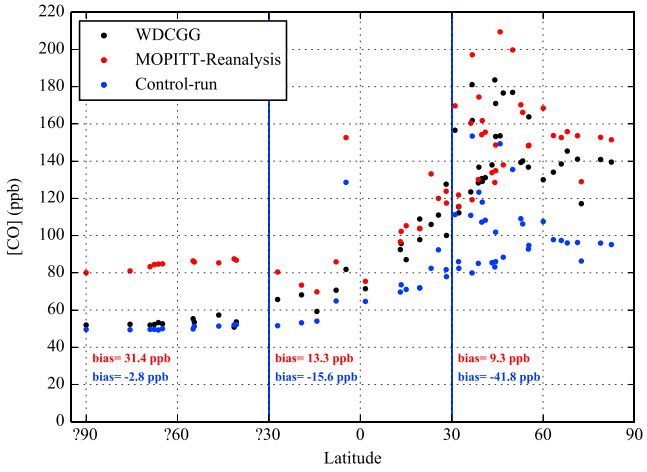

Figure 5. Annual CO average of surface WDCGG observations (black), MOPITT Reanalysis (red), and the Control Run (blue).

3.2. Evaluation Against Independent Observations

3.2.1. WDCGG Surface Observations

Annual CO mean for each WDCGG surface station and colocated averaged simulation results sorted by latitude are shown in Figure 5. The Control Run shows good agreement with the observations, capturing the latitudinal gradient with very low bias in the SH. In contrast, the Control Run underestimates CO in the NH by around 40 ppb. The increase of CO in MOPITT Reanalysis leads to an overestimation with respect to the observed values of around 30 ppb in the SH and less than 10 ppb in the NH. The high-latitude bias in the reanalysis is consistent with the findings of *Hooghiemstra et al.* [2012]

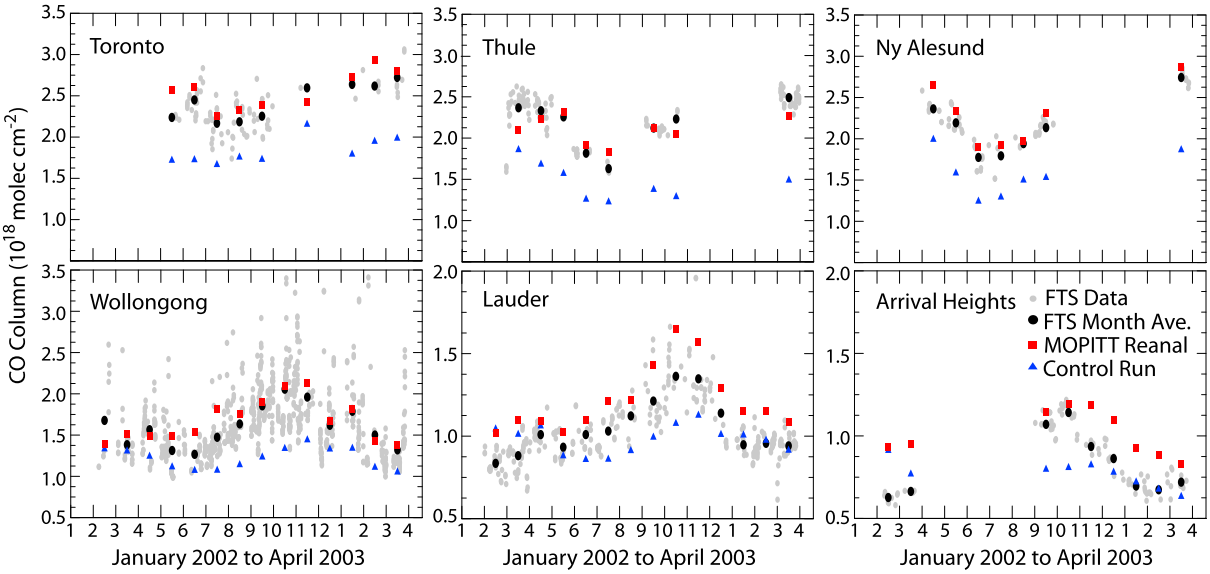

Figure 6. Comparison of CO from Control Run and MOPITT Reanalysis with monthly average NDACC-FTS retrievals at six sites. Black circles correspond to monthly NDACC retrievals of total CO columns, while the red squares and blue triangles correspond to the interpolated and smoothed profiles of CO from the reanalysis and Control Run, respectively. Ny Alesund (Norway), Thule (Greenland), and Toronto (Canada) are located in the Northern Hemisphere, while Wollongong (Australia), Lauder, and Arrival Heights (New Zealand) are located in the Southern Hemisphere. Note the different scales for Lauder and Arrival Heights compared to the other stations.

and *Jiang et al.* [2015] indicating a positive bias in MOPITT CO, in particular in the SH. However, it is important to note that the overestimation in the reanalysis is due not only to MOPITT retrieval bias but also to the model response to assimilation. A positive increment of CO in the assimilation at midlatitudes (due to MOPITT bias) can have a more important consequence on simulated CO fields if these adjusted CO plumes are transported downwind to latitudes higher than 65° because there will not be observations to constrain them. For this case, these increments can last as long as the CO lifetime, up to 3 months in polar winter, when there is no significant chemical CO loss. This is clearly seen, for instance, in CO over the South Pole Station, which was strongly affected despite the fact that no MOPITT observations were assimilated poleward of 65°S.

3.2.2. NDACC-FTS Measurements

The NDACC-FTS instruments allow a complementary evaluation at high latitudes. In the NH, we use one station close to CO sources (Toronto) and two remote stations (Ny Alesund and Thule). In Figure 6, we show the comparison of total column CO from NDACC, the Control Run, and the MOPITT Reanalysis. For the Control Run, the decrease of the total column in NH late spring is captured for all stations while the increase in NH spring 2003 is underestimated. The annual cycle is better represented in the MOPITT Reanalysis for all stations, as shown by improved temporal correlation statistics (see Table S1 in the supporting information). Although there is an overall improvement in the MOPITT Reanalysis relative to Control Run, a slight bias remains. In the SH, the Control Run reveals an underestimation of the annual CO average compared to the NDACC stations. The Control Run bias reaches −25% at the Wollongong station, which is the SH site located closest to sources. This bias is mainly driven by an underestimation of the spring peak, reaching a maximum in October at Wollongong and Lauder and in November at Arrival Heights, which is the most remote station. We see an improvement in the MOPITT Reanalysis in terms of better temporal variability and reduction in the bias over Wollongong station. However, we also see an increase in the background CO that leads to a significant bias (with opposite sign) in stations far from the sources (i.e., Lauder and Arrival Heights), consistent with the surface observations. The spring peak enhancement seen by the three SH NDACC stations is due to BB, [*Jones et al.*, 2001] suggesting an underestimation of emissions or misrepresentation of fires in the Control Run. The low bias between the Control Run and the surface observations in SH might be due to compensating effects. It is quite possible that OH in this region is too low after the assimilation or that CAM-Chem is too strongly transporting CO to the surface. It could also be that CO is uplifted to the upper layers of the troposphere with errors in plume vertical positions in CAM-Chem.

3.2.3. MOZAIC-IAGOS Measurements

CO data from MOZAIC-IAGOS were averaged over continental scales to generate vertical profiles for every season having a representative number of observations (comparable number of observations between

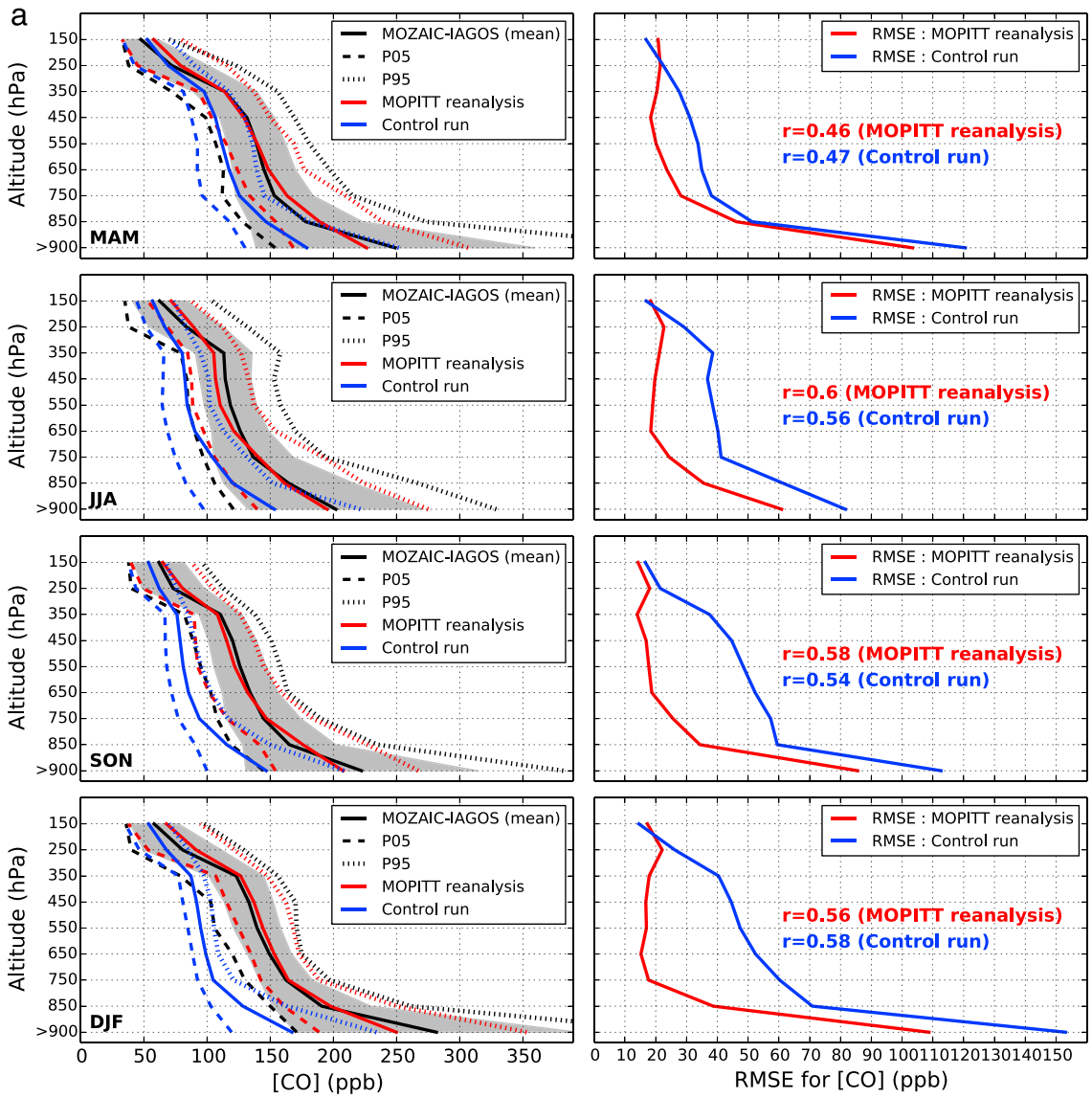

Figure 7. (a) Seasonal average CO profiles from MOZAIC-IAGOS measurements (black), MOPITT Reanalysis (red), and Control Run (blue) over the U.S./Canada region within the study period (March 2002 to March 2003). The left column shows the CO observations in black along with their standard deviation (gray). The dashed lines correspond to the 5th and 95th percentiles. The right column shows the RMSE and correlation coefficients as a function of altitude. (b) Same as Figure 7a but for Europe.

seasons). Comparison to CAM-Chem simulations is shown in Figure 7a (U.S./Canada) and Figure 7b (Europe). We note that these measurements are samples of CO from mainly three different environments. The lower level (close to the surface) is mainly representative of highly polluted conditions as can be expected over airports in large cities, such as Frankfurt, Vienna, and Munich. Most of the airports with MOZAIC-IAGOS flights in the U.S. and Canada are located in and around the Midwest (Houston, Denver, Chicago, and Toronto) and the East Coast (New York). The observed average CO is usually higher than 200 ppb for both continents with a large standard deviation and a 95th percentile that is systematically higher than 300 ppb. The resulting average RMSE can reach 150 ppb for the Control Run in winter. It is encouraging that MOPITT Reanalysis is able to improve CO in these areas despite the representation biases due to the low horizontal resolution of the model (around 2°). Both CO and its bias are decreasing with height in both simulations. However, for pressures lower than 700 hPa, CO values and errors are more homogeneous during NH summer than winter. We find a strong bias correction in the assimilation, in particular during fall and winter, for which the RMSE is lower than 20 ppb in the reanalysis. The two upper levels are located around the cruising altitude and are sampling most of the horizontal extent, which includes both the continental and oceanic background

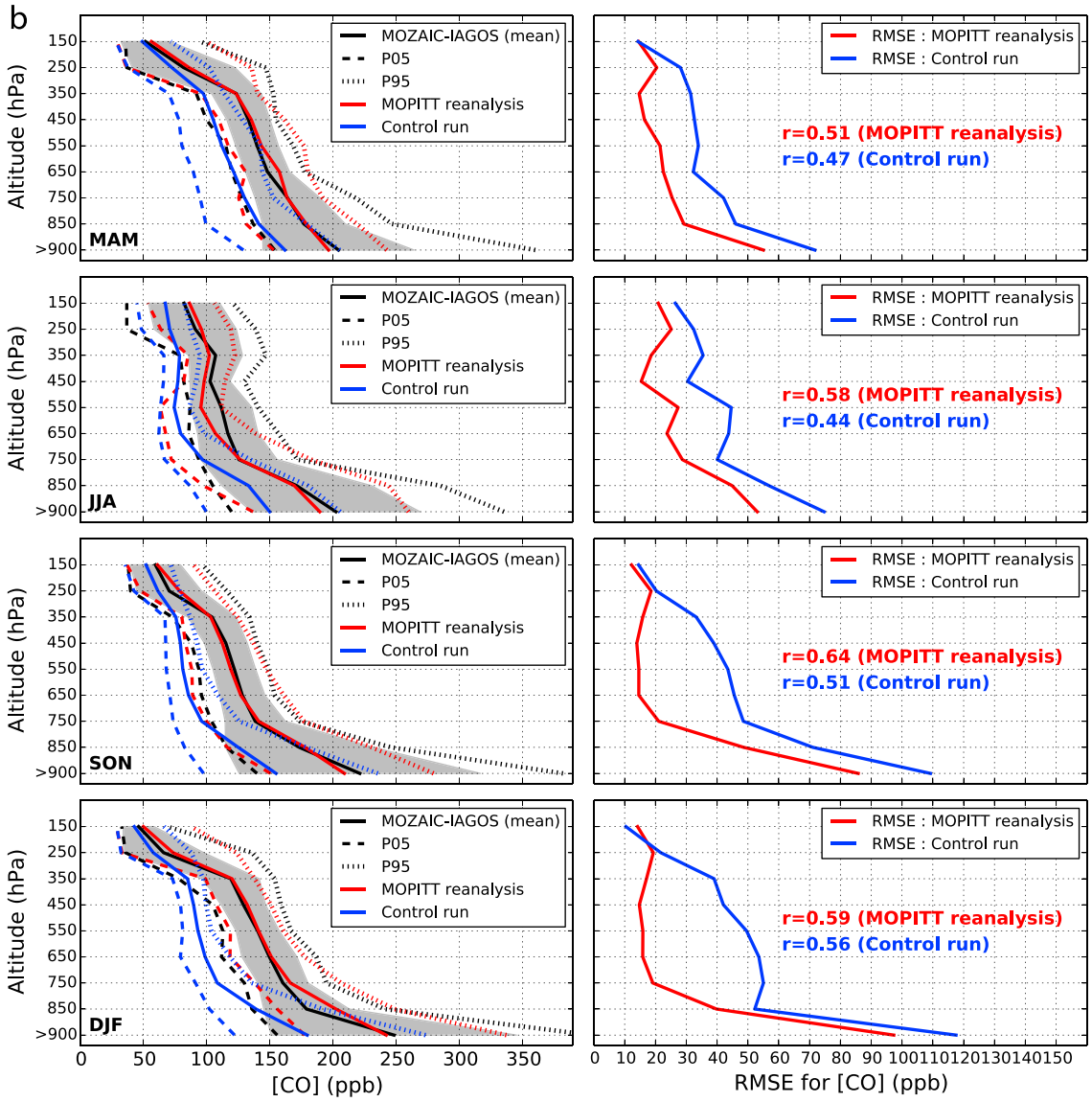

Figure 7. (continued)

(Figure 1). In this case, the Control Run exhibits a lower bias compared to MOZAIC and the improvement from the assimilation is less clear, especially for winter and spring where the RMSE is increased due to the lack of assimilated observations and a low vertical resolution near the tropopause. The correlation coefficients are usually higher for MOPITT Reanalysis than for the Control Run over North America, but slightly lower in winter and spring over Europe.

3.2.4. SMOCC Aircraft CO Measurements

Most CO measurements during the SMOCC-2002 field campaign were taken in the southern Amazon basin, a region affected by emissions from intense vegetation fires related to deforestation. This leads to large gradients between flights that were sampling the large-scale background concentrations and flights dedicated to track fire plumes. Monthly average surface CO concentrations around 500 ppb have been observed during the dry season in this region [*Fuzzi et al.*, 2007; *Artaxo et al.*, 2013]. As seen in Figure 8, there is high CO loading in combination with high spatiotemporal variability associated with burning during the dry season. A few flights into the westernmost part of the Amazon basin sampled the remote background concentrations, defined as the "green ocean" in *Andreae et al.* [2004], where the CO concentrations were still higher than 100 ppb. The RMSE of simulations is around 30 to 50% of the observed values, with a bias of up to

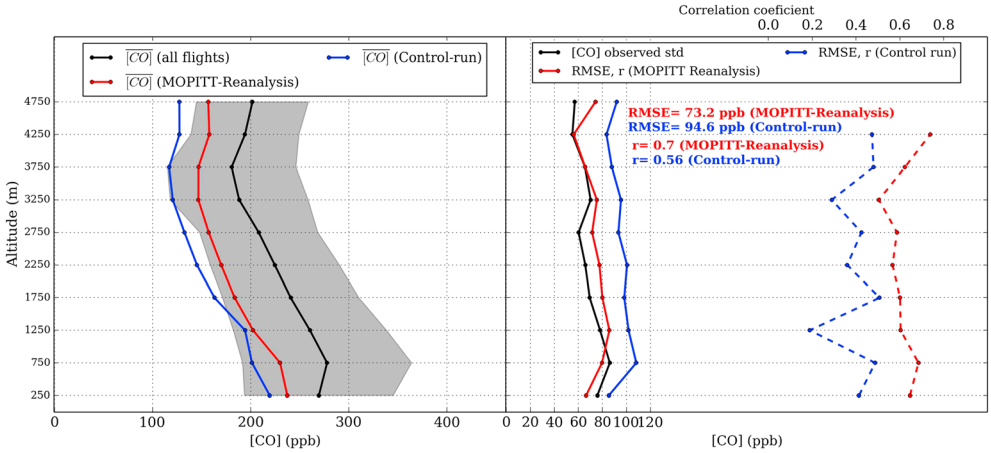

Figure 8. Statistics of simulated and observed CO profiles from all SMOCC flights averaged over (left) 500 m altitude bins and (right) the corresponding RMSE and correlation coefficients. Correlation coefficients are calculated for all data used in the study. Observations greater than 450 ppb have been removed from the analysis.

100 ppb. These results have to be compared to the observed CO variability, here measured by the standard deviation that is in the same range. The relative improvement in the MOPITT assimilation is encouraging, considering representation bias due to coarse model horizontal resolution. It shows the ability of the instrument to detect CO in the lower layers of the troposphere. This simulation should be used as a benchmark for further improvements from the modeling side, including the use of daily emissions (versus monthly), and the parameterization of the injection height and plume rise models [*Freitas et al.*, 2006; *Val martin et al.*, 2010]. However, the significant residual bias after assimilation, which is most pronounced for the flights in the smokiest regions, suggests that MOPITT observations are underestimating the CO levels in those heavily polluted conditions, as shown by aircraft data at those latitudes [*Deeter et al.*, 2013]. A bias correction of the MOPITT CO observations in these extreme conditions would improve the simulations.

In summary, our evaluation of MOPITT Reanalysis shows an overall improvement of the simulated CO fields, via removal of the winter/spring strong low bias in CAM-Chem. MOPITT Reanalysis reduces this bias to about 50 ppb in the NH. This is very consistent across all observations used in our evaluation. Far from CO source regions, the MOPITT Reanalysis is usually higher than independent observations while the bias is usually low closer to the sources. There is a positive bias in CAM-Chem as compared to MOPITT in the tropical upper troposphere that is likely due to too strong convection. Furthermore, CO is overestimated in the SH, particularly at high latitudes. We attribute this overestimation in the reanalysis to a possible bias in MOPITT and/or a systematic model error such as OH overestimation in the Control Run, but underestimation in the MOPITT Reanalysis.

4. Model Response to MOPITT Assimilation

Here we investigate the model response in CO due to the 6-hourly assimilation of MOPITT retrievals across the 1 year reanalysis period of this study. We focus on presenting the change in the chemical system in CAM-Chem (OH, O_3, CH_4, VOCs, and chemical production of CO) due to changes in modeled CO abundance by MOPITT. We begin our analysis by presenting the spatial distribution of the mean increments, which provides a perspective on the systematic adjustments by the model to match MOPITT observations. These adjustments relate to associated errors in the model representation of the processes affecting CO (transport, emissions, chemistry, and deposition). We continue our analysis by looking at key chemical species mostly affected by these CO adjustments, in particular on the changes in oxidative capacity of the troposphere and ozone production. We will then link these changes to how secondary sources of CO have been modified as a direct response to CO + OH perturbations.

4.1. CO Increments

The increments are defined as the difference between the analyzed (posterior ensemble mean) and the forecast (prior ensemble mean) fields (see equation (4)). The statistics of the increments across all observations within the assimilation period represents the systematic DA adjustment. Positive increments represent an

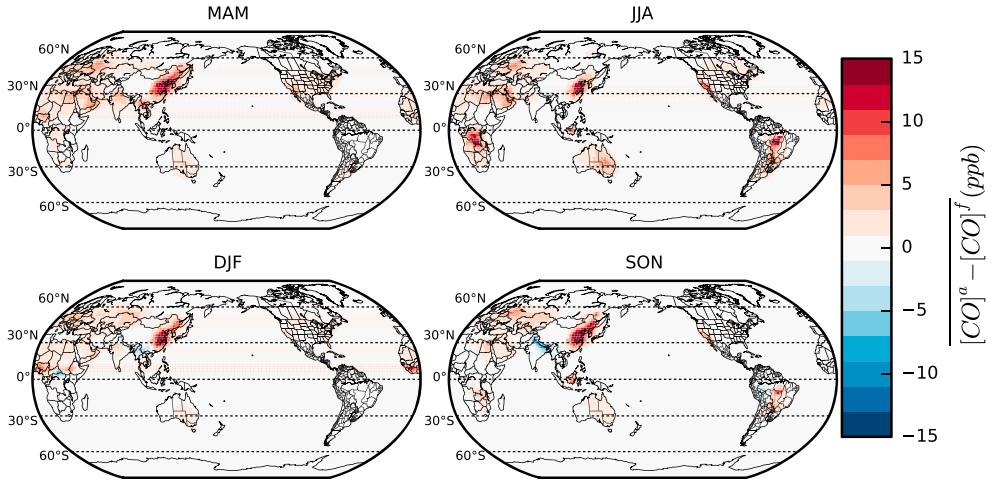

Figure 9. Mean CO increments (ppb) at the model surface across each season (MAM, SON, JJA, and DJF).

underestimation of the forecast, while negative increments represent overestimation. Most of these increments can be seen in the source regions near the surface, where errors in direct emissions are dominant. To the first order, we expect that positive increments in the model surface most likely correspond to a potential underestimation of surface emissions (as reflected by CO concentrations at this level). We note, however, that boundary layer mixing and ventilation as well as convection (especially in regions experiencing active mesoscale to synoptic weather conditions) influence model surface concentrations. Bearing this in mind, we show in Figure 9 the seasonal variation of the mean increments at the model surface level. Overall, the increments are mostly positive in areas dominated by anthropogenic and fire activities, indicative of general underestimation of our prior emissions. The largest increments occur where large fires are underestimated/overestimated (i.e., positive/negative increments in biomass burning regions in Southeast Asia, Africa, and South America) or where the prior anthropogenic emissions are underestimated (i.e., positive increments over anthropogenic source regions in East Asia, eastern Europe, and western U.S.). Several systematic patterns can also be identified across all the seasons. First, most of the increments are located on land because this is where MOPITT retrieval sensitivity is more likely to be higher in the lower troposphere (i.e., addition of near infrared in the retrieval) and provides necessary adjustments in modeled CO close to the surface. Second, eastern China, Egypt, and the Arabian Peninsula, as well as western Russia and California, have positive increments across all months suggesting an underestimation of emissions from anthropogenic sources at these locations. For most of the other increments, it is likely that they are associated with biomass burning emissions. This is confirmed by inspection of the tagged CO distributions. There is an underestimation of CO from fires for both June-July-August (JJA) and September-October-November (SON) for the Amazon forest and Indonesia, as well as western Russia, and only for JJA in the African equatorial forest and California. Fires are overestimated in Myanmar in December-January-February (DJF) and in Siberia in SON. Some situations are more complex and are likely related to transport of plumes from biomass burning, such as in northern India and over the Andes in SON.

4.2. Impact on Chemistry

The annual zonal average concentration fields for the Control Run and the MOPITT Reanalysis, as well as their relative changes, are presented in Figure 10. Differences from the Control Run represent the mismatch between MOPITT and model (in the case of CO) and between MOPITT-constrained and MOPITT-unconstrained model fields. We note here that evaluation against independent data and our inspection of assimilation diagnostics show evidence of model fit with MOPITT and other CO observations (section 3). As shown in Figure 10 (first row), the analyzed fields of CO have increased by up to 75% in the SH, on average from a background of 50 ppb to a background of 80–90 ppb relative to the Control Run. The CO increments previously shown are reflected here. We also find that there is a decrease in CO in the upper troposphere of the SH. The largest absolute increase is found in the midlatitude and high latitudes of the NH, where in the analyzed fields the background increased by around 40 to 60%, shifting from a range of 80–120 ppb to 120–160 ppb. There is also a relative increase of around 20% in the tropical upper troposphere.

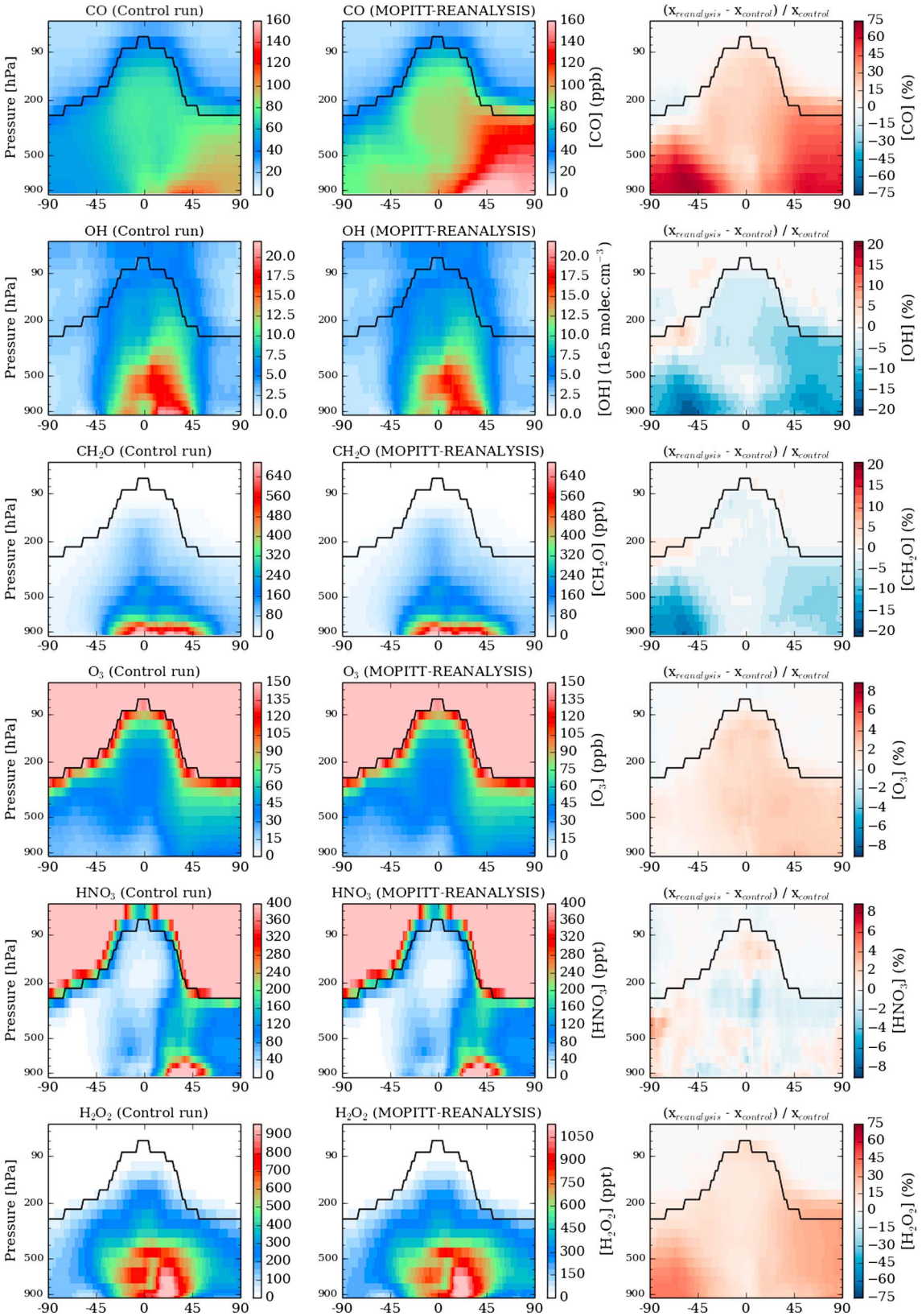

Figure 10. Latitudinal and yearly average chemical concentration fields (rows) from (left column) the Control Run, (middle column) the MOPITT Reanalysis, and (right column) the percent differences relative to the Control Run. Shown are (first row) CO, (second row) OH, (third row) HCHO, (fourth row) O_3, (fifth row) HNO_3, and (sixth row) H_2O_2. All units are in ppb, except for OH (105 molecule/cm^3). The black line indicates the chemical tropopause, defining the stratosphere when ozone is greater than 150 ppb.

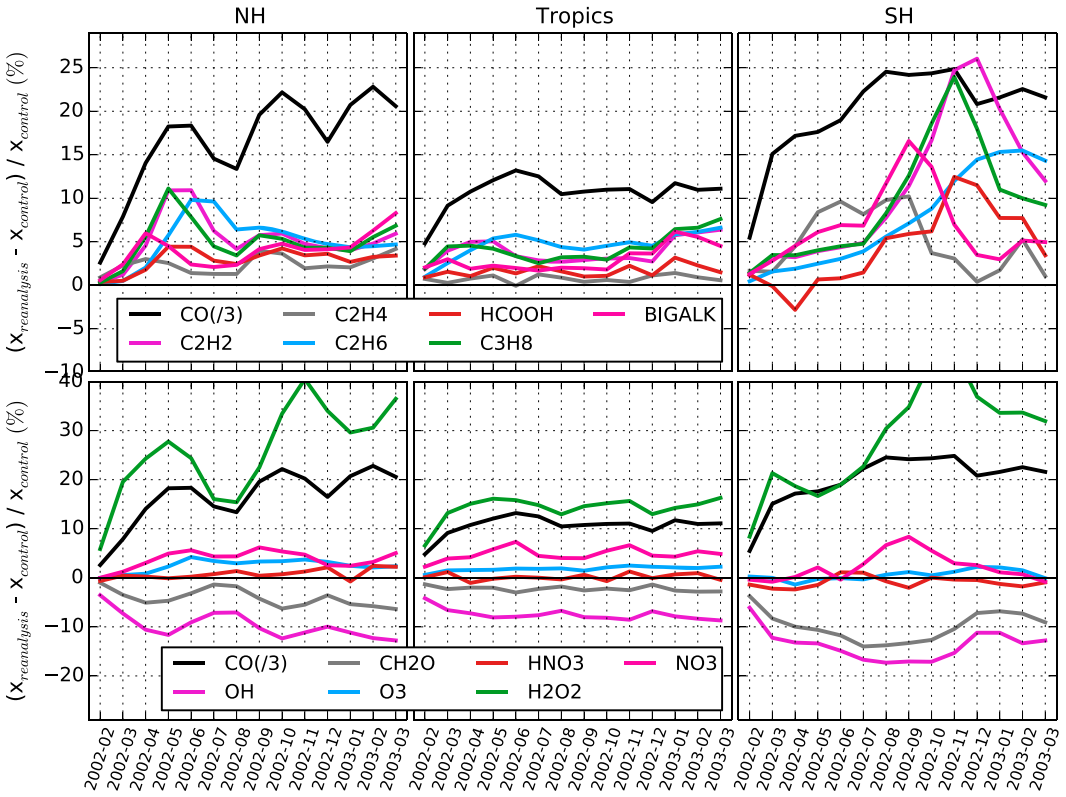

Figure 11. Monthly mean differences between MOPITT Reanalysis and Control Run for (top row) CO and NMVOCs and (bottom row) key oxidant species for the extratropical NH, the tropics, and the extratropical SH at the surface level. Note that the runs were initialized from the same fields (30 January 2002), so that the first 2 months show smaller differences due to spin-up.

The net impact of this mean CO change is a decrease in OH between 5 and 15% overall in the lower troposphere and up to 20% in the SH (Figure 10, second row). The global tropospheric mean OH reduction is 8.6%, with a reduction of 9.6% in the NH and 7.61% in the SH (Table S3). Our comparison with the TransCom OH fields [*Patra et al.*, 2011] shows a difference for the NH mean OH of 1.5×10^6 molecule/cm^3 in the Control Run and 0.76×10^6 molecule/cm^3 in the MOPITT Reanalysis (Table S3). Conversely, the SH mean OH is strongly underestimated in the Control Run (-1.27×10^6 molecule/cm^3) and in the MOPITT Reanalysis (-1.65×10^6 molecule/cm^3). This pattern of underestimation is similar to that observed by *Yin et al.* [2015], where most of the lack of OH in the SH is located in the tropics and in the middle troposphere, where the largest differences are actually close to the equator (see Figure S7). On the other hand, our OH interhemispheric asymmetry is comparable to the Atmospheric Chemistry and Climate Model Intercomparison Project (ACCMIP) multimodel estimate of 1.28 ± 0.1 [*Naik et al.*, 2013] but slightly higher in both runs (a value of 1.45 for the Control Run and 1.42 for the Reanalysis). The latest observationally derived estimate is 0.97 ± 0.12 from *Patra et al.* [2014], somehow suggesting that TransCom OH is closest to observations and that there is a missing OH source in the tropics. Overall, the overestimation of the OH asymmetry, together with the evaluation results (section 3.2), confirms an overestimation of OH in the NH and an underestimation in the SH in our experiments, which is typical of current CTMs.

The impact of CO assimilation is clearly demonstrated by these changes in OH. On one hand, the patterns in OH response are anticorrelated with the mean CO changes as the CO + OH reaction is the primary loss mechanism for OH. The only OH increase is seen in the upper troposphere of the SH, where CO has decreased. On the other hand, the changes in OH have further nonlinear effects on the other species. First, the reduced OH limits the oxidation of VOCs and CH_4, thus reducing the HCHO concentration by around 5–10% and 10–20% in the SH (Figures 10 (third row) and 11). The spatial pattern in significant HCHO changes is very similar to OH, with most notable changes in the midlatitude to high latitudes. In low NO_x conditions, HO_2 reacts to form H_2O_2, which has increased by up to 50% and shows similar patterns to the OH changes

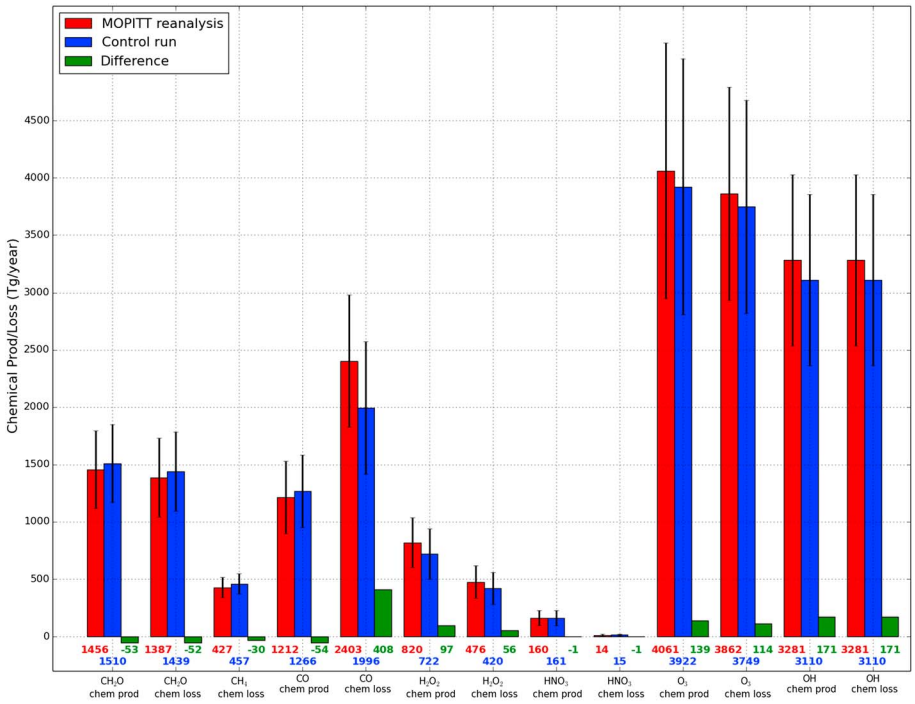

Figure 12. Annual chemical production (*P*) and destruction (*L*) of key species in the chemical troposphere (in Tg/yr). Error bars correspond to the ensemble standard deviation. Values are indicated below the bar plot. Differences are calculated as MOPITT Reanalysis minus Control Run.

(Figure 10, sixth row). Despite the fact that H_2O_2 can be photolyzed back to OH, its formation is a loss to the HO_x family, meaning that part of the OH loss by the increase in CO will not be available for VOC and CH_4 oxidation [*Seinfeld and Pandis*, 1998]. Conversely, there is ozone formation if the HO_2 (formed by CO oxidation) is recycled back to OH by NO_x, which leads to HNO_3 formation. Differences in the HNO_3 fields are small because of the rapid loss by wet deposition (Figure 10, fifth row). However, there is a significant increase in O_3 in regions where NO_x is at sufficient levels to effectively produce O_3, as can be seen especially in the NH and in the tropics. There, the net increase is around 5%, whereas no significant changes are observed in the SH (Figure 10, fourth row).

To further illustrate these changes, we show in Figure 11 the changes due to MOPITT assimilation in the chemical fields at the surface over time and averaged over the NH, tropics, and SH regions due to MOPITT assimilation. This is represented here as the percentage difference between the MOPITT Reanalysis and the Control Run relative to the Control Run. The NMVOCs listed on the first row (acetylene (C_2H_2), ethylene (C_2H_4), ethane (C_2H_6), propane (C_3H_8), and BIGALK which represents alkanes C_4 and larger) are directly emitted and are not chemically produced in the atmosphere. The main sink of these species is in the form of OH abstraction. Hence, their concentrations are sensitive to the reduction in OH. Consequently, concentrations of these species are increased, especially during the respective spring and summer of the NH and SH seasons. We also show the time series for HCOOH (which is the simplest carboxylic acid) and H_2O_2. Oxidation through $RO_2 + HO_2$ is more favored since OH is converted to HO_2 by CO + OH reaction. HO_2 can also react with itself to produce H_2O_2. We find that both H_2O_2 and HCOOH are increased due to more HO_2. Conversely, the lower CH_4 and NMVOCs chemical oxidation rate (due to lower OH) leads to a reduced chemical production of HCHO (emissions are the same in both runs). The cycling of HO_x in the presence of NO_x should explain the slight increase in ozone in the MOPITT Reanalysis. As shown in Figure 11, there is relatively little change in HNO_3, but there is an increase in NO_3, suggesting a higher oxidation stage for NO_x in the MOPITT Reanalysis.

In order to evaluate the processes involved in the changes presented in Figures 10 and 11, we also calculated the integrated chemical production and destruction rates for CO, HCHO, O_3, OH, H_2O_2, and HNO_3, as well as the CH_4 destruction rate. This is shown in Figure 12, which helps explain the nature of the changes of the chemical fields.

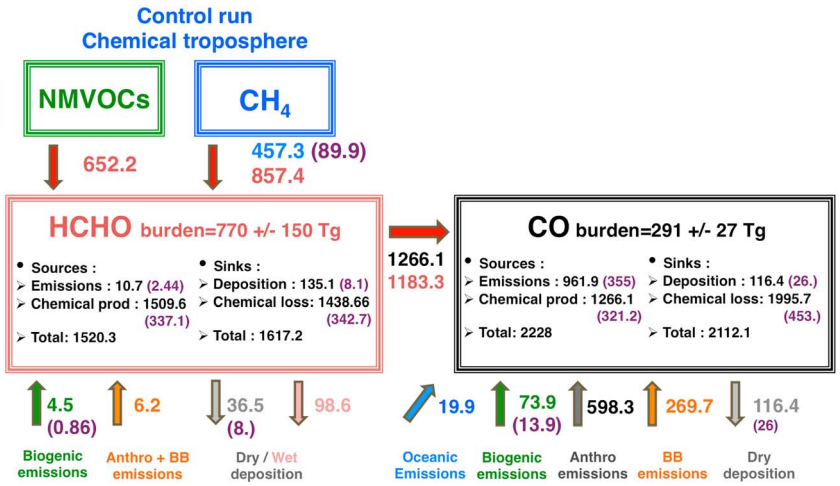

Figure 13. CO and HCHO annual budget (Tg/yr) in the chemical troposphere for the Control Run. The CO chemical production is assumed to be due to formaldehyde oxidation. The NMVOC oxidation is deduced from the difference between the total chemical production of HCHO minus the production of HCHO from CH_4 oxidation. The ensemble standard deviation is indicated in parentheses. Note that the spread in the nonbiogenic emission fluxes is calculated from the prescribed values (40%; see section 2.3.1).

As discussed earlier, the CO loss is caused by its oxidation with OH. The initial chemical model response due to higher CO concentrations is an increase in the CO loss and correspondingly in OH loss (Figure 12). Changes in OH lead to further response depending on the dominant chemical pathways and concomitant photochemical regime. In the presence of NO_x (e.g., in the NH), it leads to an increase in O_3 chemical production and consequently slightly enhanced O_3 concentrations (see also Figures 10 and 11). However, ozone photolysis (O_3 loss) will also lead to OH production in the presence of water vapor. Consequently, the observed higher O_3 loss (Figure 12) can be explained by the increase in the OH chemical production (more recycling), which compensates for the initial response of increased OH loss. In the absence of NO_x, however, the $HO_x = (OH + HO_2)$ species are converted to H_2O_2, leading to higher H_2O_2 concentrations (e.g., in the high-latitude SH) (Figure 11) and higher chemical production (Figure 12). This pathway is considered a net loss mechanism for HO_x. As a consequence of this overall OH loss, we find lower CH_4 loss and correspondingly lower HCHO production (Figure 12), as well as lower HCHO concentrations (Figure 11) leading to lower CO chemical production (Figure 12). This can be seen clearly in the low NO_x regions of the Southern Hemisphere, where there is no significant change in O_3 concentrations even with enhanced CO. Globally, the increase in CO burden with MOPITT assimilation leads to a higher O_3 chemical production, a net reduction in OH concentration, and subsequent reductions in CH_4 oxidation, and CO chemical production. We note that CH_4 surface concentrations are prescribed in our reanalysis. Hence, the impact of CO adjustments to CH_4 distribution is expected to be minimal. However, we can further elucidate the indirect impact through the decrease in CH_4 oxidation (loss due to OH).

It is worth mentioning here that the effect of CO assimilation on the chemical system is highly nonlinear and centered around changes in the OH sink, which then feeds back to the OH source processes depending on the chemical regime (HO_x recycling). While the changes in OH appear to provide a positive impact in NH, the underestimation of OH in the SH is exacerbated by assimilation due to MOPITT bias (to the first order). Independent evaluation of other species (not shown) reveals that the chemical system has been either significantly degraded or improved. One of the goals of this paper is to elucidate the changes in the chemical system and point out these nonlinearities, which can only be addressed (based on this study and supported by literature) through either constraining OH and/or the main factors affecting its cycle (not just its sink with CO).

4.3. Global CO Burden

In order to complete the evaluation of the model response to the MOPITT CO data assimilation, the CO and HCHO annual global tropospheric budget is elucidated further in Figure 13 for the Control Run and Figure 14

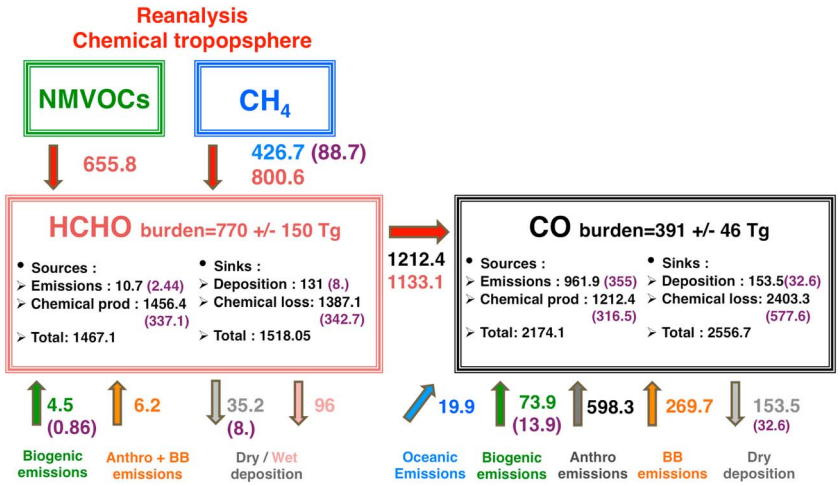

Figure 14. Similar to Figure 13 but for MOPITT Reanalysis.

for the MOPITT Reanalysis and in Table S2. This represents a schematic representation of the main "reservoirs" and "fluxes" affecting CO, similar to the figures in *Fortems-Cheiney et al.* [2011, 2012] and *Yin et al.* [2015]. Overall, the global magnitudes of each component controlling the burden of CO (in both control and reanalysis) are within the range of values reported in the literature (i.e., emission ~40% and chemical production ~60% from which ~60% is due to CH_4 oxidation) [e.g., *Duncan et al.*, 2007; *Stein et al.*, 2014]. As expected, OH dominates CO loss followed by a much smaller extent (~5%) by CO dry deposition. Here we note that the ensemble standard deviation was derived as a result of either prescribed noise on emissions and CH_4 or from the model response and coupling, which propagates the noise from the meteorological assimilation and emissions perturbations. For example, for a range of standard deviation between 10% (CH_4) and 40% (CO) of perturbations that we added in the emissions, together with the spread stemming from meteorological perturbations, the ensemble run generated a spread of around 10% for the CO burden and 20% for chemical production.

The comparison of the budget between MOPITT Reanalysis and the Control Run (Figures 13 and 14) confirms some of the findings described earlier. The HCHO burden is reduced from 770 to 742 Tg, because of a reduced chemical production (conversion of NMVOCs + CH_4 to HCHO is reduced from 1510 to 1456 Tg/yr HCHO). This decrease translates into a decrease in the chemical destruction (less VOC source of OH recycling). Note that the response to OH is mostly seen in the oxidation of CH_4 rather than that of NMVOCs. As a consequence, CO chemical production (secondary CO) is decreased by ~54 Tg/yr CO (from 1266 to 1212 Tg/yr CO) (see Figure 12 as well). However, the global CO burden has increased by 100 ± 53 Tg CO (from 291 to 391 Tg CO) as an overall response to MOPITT assimilation. This increase in burden can be seen in the increase of CO loss by 20% and dry deposition by around 30% (both of which are directly related to the CO burden). The apparent lack of mass (CO burden) in the Control Run (25% lower than in the MOPITT Reanalysis) can be attributed to an underestimation of CO sources from chemical production and/or direct emissions. In the case of chemical production, this underestimation can be due to CAM-Chem strongly underestimating NMVOCs [e.g., *Emmons et al.*, 2015]. Our limited evaluation with NDACC shows an underestimation of C_2H_6 by a factor of 2. The underestimation of chemical production can also be partly due to the apparent overestimation of wet deposition in CAM-Chem. There is a significant loss in CO of around 6% (9% for the total) through wet deposition of HCHO and other oxygenated species like $HOCH_2OO$ and HCOOH. The yield of CO production from HCHO in CAM-Chem is ~75% (1133 Tg/yr CO from HCHO/1518 Tg/yr HCHO) for the MOPITT Reanalysis. A similar yield of ~73% is found for the Control Run. This is significantly lower than previous results indicating that the model wet deposition in CAM-Chem is higher than in previous studies and is not negligible (e.g., 100% in *Duncan et al.* [2007]). Bearing this in mind, attributing the change in CO burden as a response to MOPITT assimilation to underestimation of direct emissions alone is misleading due to the nonlinearity of the system. This has been alluded to and reported indirectly in past studies [*Jiang et al.*, 2011, 2015]. Here we show direct evidence of this CO-OH-CH_4 feedback.

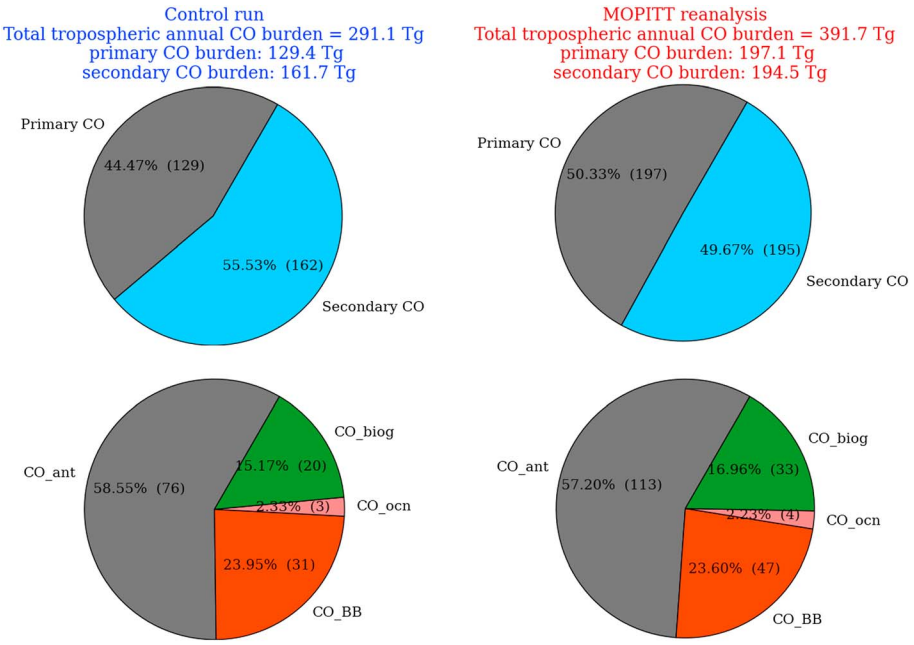

Figure 15. The CO annual tropospheric burden composition (Tg/yr) is presented for (left column) the Control Run and (right column) the MOPITT Reanalysis. (top row) The fraction of primary versus secondary CO. (bottom row) The sources contribution to the primary CO burden.

We further elucidate this point by conducting a mass balance using the burden of our updated CO tags and the total burden from the Control Run and MOPITT Reanalysis (see Figure 15). Based on CO tags, the primary CO burden increased by about 50% (from 129 Tg CO in the Control Run to 197 Tg CO in the MOPITT Reanalysis) as a result of MOPITT assimilation. We infer the secondary CO burden from the difference between the total and primary CO burden (both of which were constrained by MOPITT in MOPITT Reanalysis). This has increased by 20% (from 162 Tg CO in the Control Run to 195 Tg CO in the MOPITT Reanalysis) due to MOPITT assimilation. Secondary CO needs to be increased in spite of the fact that chemical production of CO from CH_4 and NMVOCs has decreased by 54 Tg CO/yr as a response to a decrease in OH due to MOPITT assimilation. This points to the impact of constraining secondary CO in the CO budget and the role of understanding the CO-OH-CH_4 feedback in improving the accuracy of emission estimates. We supplement the results of past studies, such as *Jiang et al*. [2011] and *Fortems-Cheiney et al*. [2012], by presenting direct evidence of this nonlinearity.

The partitioning between primary and secondary CO has slightly change from 44.5% and 55.5% in Control Run to 50% and 50% in MOPITT Reanalysis. If we look at the seasonal burden (not shown), it suggests that the partitioning varies in the MOPITT Reanalysis from 44% of primary origin in JJA to 55% in DJF while a maximum CO burden of 420 Tg is found in SON, due to an increased BB contribution. The biogenic CO burden, for which emissions are estimated using MEGAN, is increased from 20 in the Control Run to 33 Tg in the MOPITT Reanalysis (Figure 15). This suggests that either VOCs from MEGAN or their chemical fate is underestimated. This could imply a deficiency of secondary CO in both model simulations.

5. Discussion

Our evaluation of analyzed CO fields in section 3 points to a relatively important overestimation of the analyzed CO background in the SH extratropics by around 30 ppb. This result is consistent with *Hooghiemstra et al*. [2012], who found an overestimation of 20 ppb by inverting emissions using MOPITT v4. For those latitudes, the CO measured at surface stations is somehow representative of the tropospheric burden (i.e., remote and well-mixed regions). The CO burden for this region is 54.5 Tg for the Control Run and 77 Tg for the MOPITT Reanalysis. CO is underestimated by around 2.8 ppb (5%; see Figure 5) relative to mean observation value of 53.2 ppb. If we adjust the SH burden by 5% (which gives 57.3 Tg), this new estimate appears to

correspond to the increase in the BB burden seen in the MOPITT Reanalysis (sections 4.1 and 4.3). We propose that the estimate of the SH burden should be 57.3 Tg instead of 77 Tg (MOPITT Reanalysis), based on the corrected Control Run burden. This adjustment in the CO budget will result in a total tropospheric burden for the analyzed year of 371 Tg CO as opposed to 391 Tg CO. The uncertainty on the total tropospheric burden estimated using the ensemble spread in the reanalysis is 12%.

The evaluation of the differences between CO abundance as optimized by data assimilation (MOPITT Reanalysis) and the Control Run indicates an underestimation of both emissions and chemical production of CO. It should be noted that the emissions are not directly estimated in the assimilation but are inferred from the CO burden of the CO tags, which were also constrained by MOPITT (see section 2.3.2). We recognize, however, that there is a potential influence of the distribution of our a priori emissions on this inference (even in a global sense). Hence, only the following partial conclusions can be drawn on emission adjustments based on the adjustments in CO abundance (state estimation):

1. The underestimation of anthropogenic emissions explains some of the CO bias in CAM-Chem, as suggested by inversion studies. This underestimation can be up to 50% of the observed values and may be even more significant in terms of regional differences. The increments (due to MOPITT assimilation) suggest a large underestimation over East Asia, although errors from Europe and U.S. CO emissions cannot be disregarded, for instance, errors coming from traffic emissions [*Stein et al*., 2014].
2. The BB emissions of CO and VOCs, their chemical reactivity, and their transport play a dominant role in JJA and SON. Most of them occur in the tropical band, defined here as between 30°S and 30°N, where nearly half of the global CO burden resides (200 Tg out of 371 Tg). Our findings of a potentially too strong vertical mixing in CAM-Chem and subsequent chemical response indicate the importance of model errors in particular for that region [*Jiang et al*., 2015; *B2015*].
3. The CO biogenic tag suggests that biogenic emissions or associated VOCs that oxidized quickly to CO may be underestimated.
4. Once again, we highlight that the underestimation of the secondary CO is at least as important as the primary emissions. This demonstrates that chemistry is central in the CO error budget.

We also find that tropospheric CH_4 lifetime (which has been derived for both experiments) has also changed. While the CH_4 burden has remained fairly constant (as can be expected since CH_4 concentrations are prescribed in both runs), CH_4 loss has decreased by 30 Tg/yr (from 457 ± 90 Tg/yr CH_4 in Control Run to 427 ± 89 Tg/yr CH_4 in MOPITT Reanalysis; see Table S2 as well). This leads to an increase in lifetime by around 6 months from 8.7 ± 0.22 years in the Control Run to 9.3 ± 0.23 years in the MOPITT Reanalysis. The values of the Control Run (8.7) are consistent with the study by *Tilmes et al*. [2015] reporting a similar range of results by assimilating the meteorology (specified dynamics). However, the CH_4 lifetime from reanalysis is significantly closer to the Atmospheric Chemistry and Climate Model Intercomparison Project (ACCMIP) multimodel mean of 9.7 years [*Naik et al*., 2013] and to observation-based estimates of the CH_4 lifetime of 10.2 [*Prinn*, 2005] and 11.2 [*Prather et al*., 2012] years.

Finally, we investigated in this study the chemical response from the assimilation of the CO state only, using an ensemble of forward coupled chemistry transport simulations, with a full tropospheric gas chemistry mechanism and a simple aerosol model. Emissions and other chemical concentrations or fluxes were not optimized during the CO update. The first-order chemical feedback, i.e., the oxidation by OH, seems to be improved by the CO assimilation, as indicated by the CH_4 lifetime. Comparison with TransCom OH fields reveals that this improvement is seen in the NH. The decrease in OH should theoretically increase the CO lifetime and therefore its abundance. It appears that it leads to an increase of tropospheric ozone in favorable conditions. This can enhance the photochemical production of OH, which is a negative feedback. However, this is not the case in the SH were MOPITT bias further degrades the OH fields (relative to TransCom). This highlights the need for bias correction in assimilating these retrievals and additional constraints on OH.

The formation of HCHO from CH_4 and NMVOCs falls within the latest state-of-the art estimates, if we consider that all produced HCHO would have formed CO. For the Control Run, the chemical production of HCHO from CH_4 is 857 Tg/yr (which would lead to 801 Tg/yr of CO), compared to 800 Tg/yr of CO from *Prather et al*. [2001] and a multimodel mean of 766 Tg/yr [*Shindell et al*., 2006]. We deduce a chemical production of HCHO of 652 Tg/yr (which would lead to 609 Tg/yr of CO), compared to a multimodel mean of 730 Tg/yr [*Shindell et al*., 2006]. The reduced OH leads to an increased lifetime of NMVOCs (and CH_4). As a result, there is an

increase in the loss of HCHO. The loss of intermediate oxygenated NMVOCs through wet and dry deposition is responsible for a reduced CO secondary formation. The overall CO chemical production in the MOPITT Reanalysis is 1266 Tg/yr. Since the CO chemical production is down to 1212 Tg/yr, an overall increase of CO by assimilation leads to a decrease of CO chemical destruction. The multiple pathways and especially the formation of more oxygenated species, more subject to wet deposition, does not favor CO production. As noted by *Stein et al*. [2014], the use of another dry deposition scheme led to a 14 Tg increase of the CO burden.

6. Conclusions and Future Directions

One year of daytime multispectral MOPITT retrievals of CO partial columns have been assimilated in the coupled chemistry-climate model CESM/CAM-Chem. This is part of an ongoing decadal chemical reanalysis project at the National Center for Atmospheric Research using the same ensemble-based data assimilation system that was previously applied for chemical weather studies which adopted a newer DA approach of joint assimilation of meteorological and CO observations. Here we presented the results of the initial year of reanalysis with a particular focus on two objectives: (a) reevaluating the CO distribution constrained by MOPITT over a period beyond weekly monthly variations as was done in our previous chemical weather studies and (b) elucidating the changes in the chemical system as a response to the changes in CO abundance due to the assimilation of MOPITT. We note that this reanalysis only optimizes the meteorological and CO states in CESM (i.e., emissions are prescribed). Our goal is to provide a best estimate of the CO spatiotemporal distribution for future applications. We have taken this approach to gain insights on the key drivers of CO variability as well as uncertainties in modeling the chemical system otherwise obfuscated by confounding factors and nonlinearities.

Overall, our diagnostics of MOPITT data assimilation demonstrate an efficient assimilation and a well-balanced global error budget. Our global evaluation based on four different independent sets of measurements shows that the best improvements in CO distribution are found when the simulation errors are the greatest (i.e., during spring) and when the MOPITT V5J observations are the most sensitive and accurate, i.e., in the lower/middle troposphere over land. This is especially shown in our comparison with MOZAIC profiles. We find that certain adjustments in CO during assimilation of MOPITT can be transported to downwind areas not directly sampled by MOPITT. This leads to important corrections in the transport of high CO from possibly missing fire events in our prior emission inventory. Such corrections may not be found when optimizing emissions alone (e.g., CO source inversion). In addition, the seasonal cycle of CO has been improved in the MOPITT Reanalysis. We find, however, an exaggerated increase of CO at high latitudes (in particular during winter and in the SH) which we attribute to a combination of missing CO sink and bias in MOPITT retrievals. Over East Asia and Russia, we find a bias across all seasons. On the other hand, we also find that the MOPITT retrievals over the Amazon might be too low, or poorly sampled for fires, leading to a residual underestimation of CO compared to SMOCC aircraft in situ measurements. At the surface, the mean of CO increments due to assimilation indicates systematic errors, most likely to be missing fire emissions. In fact, we find that BB sources are underestimated on average in the Amazon, equatorial Africa, and Indonesia. This is complicated, however, by potentially too strong convection in the tropics leading to a bias in the upper levels of the troposphere in these regions.

Our assimilation of MOPITT in CESM/CAM-Chem resulted in key adjustments in the chemical system, primarily elucidating the nonlinearities in species abundance with OH radical concentrations. We estimate the total tropospheric CO burden in 2002 (from ensemble mean and spread) to be 371 (±12%) Tg for MOPITT Reanalysis and 291 (±9%) Tg for our reanalysis with no MOPITT assimilation (Control Run). While direct emissions of CO appear to be low, our analysis of the CO burden suggests significant contributions from hydrocarbon oxidation despite a modest decrease in secondary CO flux resulting from the model chemical response to the increase in the CO burden with MOPITT assimilation. In general, we see an improvement in simulated OH due to changes in CO as a result of assimilation especially in the NH. We find an improved CH_4 lifetime of 9.3 years in the MOPITT Reanalysis instead of 8.7 years in the Control Run, suggesting that OH is too high in our Control Run.

This is further illustrated by comparison with TransCom OH, suggesting an improvement in the simulated OH in the tropical NH. The same comparison also reveals an underestimation of OH in the tropical SH (which is

typical of current CTMs). Assimilating MOPITT in CAM-Chem exacerbates the CO bias in the extratropical SH. This implies the inability of the modeling system to generate OH, which would compensate for the CO increase due to the potential MOPITT bias in this region. We note, however, that this CO bias has only a modest impact on the CH_4 lifetime and global CO burden, since most of CH_4 and CO burden and chemical fluxes occur in the tropics and in the NH. A recent study suggests that complementary recycling pathways of OH can be substantial in pristine environments and should be considered in this context [*Lelieveld et al*., 2016].

We also find that positive correlation between ozone and CO in the presence of NO_x leads to an increase of ozone in the NH. As a result, the positive ozone bias in the model is increased by this ozone enhancement. Another consequence of this increase, however, is enhanced photochemical activity that can eventually lead to a more efficient (albeit likely overestimated) OH production. However, we also find that the secondary CO formation from CH_4 might be underestimated in both experiments despite the relatively high OH in the NH in the model. CO production from CH_4 and VOCs is lower than previously published estimates, likely because intermediate oxygenated species can be lost through wet deposition. It is found that the yield of CO production from HCHO is 75%, suggesting that the overall efficiency of CO production from CH_4 might have been overestimated in previous studies. These cascading (and compensating) effects illustrate the nonlinearities in the modeled chemical response and suggest that some model parameters should be adjusted during assimilation to provide a more consistent forecast. We advocate that these physical and chemical processes are important and need to be taken into account (as opposed to using linear and simplified schemes) and further research needs to be done to fully characterize the CO budget (both primary and secondary). As noted in *Strode et al*. [2015], biases in OH, CO emissions, and transport are not mutually exclusive, and the model bias in CO is likely to be a combination of these factors.

Within the context of chemical reanalysis, our results point to key modeling and analysis considerations, especially in improving the accuracy and consistency of our estimates of chemical fluxes as a result of the interplay between emission, transport, chemistry, and deposition processes. We suggest the following future directions from this work:

1. Accounting for model errors to improve not only the magnitude but also the structure of the ensemble statistics (error covariance) is important. For example, there is opportunity in a coupled modeling system to use different physical parameterizations for vertical convection and/or for dry and wet deposition. In addition, errors in model forcings can be applied within the ensemble framework (e.g., use of different land use for biogenic emission and deposition and different emission models and inventories). While we have partially shown this from the spread of biogenic emissions and deposition rates, elucidating these benefits comprehensively is a necessary first step.
2. Although we employ a variable localization in our current assimilation approach, there is opportunity to take advantage of the meteorology/chemistry coupled system in the future. Use of correlated information of meteorological, chemical, and physical variables, which can be observed, might aid in improving the consistency of the full initial conditions. We note, however, that careful implementation (i.e., use of specific localization length due to model error and sampling noise) needs to be conducted. For CO, further research needs to be done regarding the state/parameter/fluxes to be estimated (e.g., CO states, emissions, surface fluxes, secondary CO, as well as the state, emissions, and deposition fluxes of CO precursors like HCHO or NMVOCs). This is to ensure consistency in the estimates of the chemical system. In particular, better determination of VOC oxidation steps could be improved by careful use and understanding of HCHO data and related biogenic emissions [*Marais et al*., 2012; *De Smedt et al*., 2015]. For ozone, the use of state augmentation, with a careful way of minimizing sampling errors, may address nonlinear effects since errors and chemical feedbacks are negatively correlated [*Zoogman et al*., 2014]. The use of CO and O_3 error correlations in conjunction with collocated observations can also improve both CO and O_3 spatiotemporal distribution and budgets [e.g., *Barré et al*., 2013].
3. Including more processes in the model would allow the perturbation of CO and OH to change the formation of secondary aerosols, the oxidation of VOCs [e.g., *Hodzic and Jimenez*, 2011], and cloud chemistry. For instance, a recent study on the sensitivity of BB emissions shows that the reduced OH availability in fire plumes leads to a different yield of aerosol formation from (biogenic) isoprene [*Daskalakis et al*., 2015]. Moreover, *Mao et al*. [2013] proposed a catalytic mechanism that converts HO_2 to H_2O instead of H_2O_2 through its uptake on aerosols that leads to a reduced OH level and thus diminishes the CO bias. An

improved aerosols scheme could help in better determination of the OH fields, while CO assimilation can inform about aerosols related to combustion [e.g., *Arellano et al*., 2010; *Konovalov et al*., 2011].

4. The use of optimized CO emissions or analyzed fields of CO or even a multispecies assimilation could help obtain an improved tridimensional distribution and a better seasonality of OH for CH_4 inversions. The saved OH can be used to force CH_4 simulation as suggested in *Strode et al*. [2015]. Initial multispecies inversions and assimilations demonstrate some synergies between different observations [*Butler et al*., 2005; *Pison et al*., 2009; *Miyazaki et al*., 2015]. The assimilation can also be complemented by the use of IASI in combination with MOPITT [*Fortems et al*., 2009; *Inness et al*., 2013; B2015]. A bias correction strategy should be utilized to fully employ measurements from these instruments.
5. Recently developed advanced data assimilation algorithms that are designed to handle nonlinearities, as well as parameter estimation and bias correction, such as the Modified Restart EnKF [*Song et al*., 2014] and the Iterative Ensemble Kalman Smoother [*Bocquet and Sakov*, 2014], show great potential to provide a more robust chemical data assimilation performance.

Notation: List of Acronyms

ACARS	Aircraft Communications and Reporting System.
AIRS	Atmospheric Infrared Sounder.
BAM	bulk aerosol model.
BB	biomass burning.
BF	biofuel.
CAM-Chem	Community Atmosphere Model with Chemistry.
CESM	Community Earth System Model.
CICE	Community Ice Code.
CLM	Community Land Model.
CTM	Chemical Transport Model.
CAMS	Copernicus Atmosphere Monitoring Service.
DA	data assimilation.
DART	Data assimilation Research Testbed.
DFS	Degree of Freedom for Signal.
EAKF	Ensemble Adjustment Kalman Filter.
EnKF	Ensemble Kalman Filter.
ECMWF	European Center for Medium-Range Weather Forecasts.
EOS	Earth Observing System.
FINN	Fire Inventory from NCAR.
FF	fossil fuel.
FTS	Fourier transform spectrometer.
FV	finite volume
GC	Gaspari and Cohn.
GMD	Global Monitoring Division.
IAGOS	In-Service Aircraft for a Global Observing System.
IASI	Infrared Atmospheric Sounding Interferometer.
IFS	Integrated Forecasting System.
LMDz-SACS	Laboratoire de Météorologie Dynamique model with Zooming capability-Simplified Atmospheric Chemistry System.
MACC	Monitoring Atmospheric Composition and Climate.
MEGAN	Model of Emissions of Gases and Aerosols from Nature.
MLS	Microwave Limb Sounder.
MOPITT	Measurement of the Pollution in the Troposphere.
MOZAIC	Measurement of Ozone and Water Vapor by Airbus In-Service Aircraft.
MOZART	Model for Ozone and Related chemical Tracers.
NASA	National Aeronautics and Space Administration.
NCAR	National Center for Atmospheric Research.

Acknowledgments

The authors acknowledge the strong support of the European Commission, Airbus, and the Airlines (Lufthansa, Air France, Austrian, Air Namibia, Cathay Pacific, and China Airlines so far) who carry the MOZAIC or IAGOS equipment and perform the maintenance since 1994. MOZAIC is presently funded by INSU-CNRS (France), Météo-France, CNES, Université Paul Sabatier (Toulouse, France), and Research Center Jülich (FZJ, Jülich, Germany). IAGOS has been and is additionally funded by the EU projects IAGOS-DS and IAGOS-ERI. The MOZAIC-IAGOS data are available via CNES/CNRS-INSU Ether website http://www.pole-ether.fr. The data used in this publication were obtained as part of the Network for the Detection of Atmospheric Composition Change (NDACC) and are publicly available (see http://www.ndacc.org). The NCAR FTS observation program at Thule, Greenland, is supported under contract by the National Aeronautics and Space Administration (NASA). The Thule project is also supported by the NSF Office of Polar Programs (OPP). We wish to thank the Danish Meteorological Institute for support at Thule. The FTS measurements and analysis at Toronto were supported by NSERC, the Canadian Space Agency, and Environment Canada. The measurement program at Wollongong has been supported by the Australian Research Council for many years, most recently by grants DP110101948 and LE0668470. SMOCC was funded by the European Commission, the Max Planck Society, the Fundacão de Amparo à Pesquisa do Estado de São Paulo, and the Conselho Nacional de Desenvolvimento Científico (Instituto do Milênio LBA). Computing resources were provided by the Climate Simulation Laboratory at NCAR's Computational and Information Systems Laboratory (CISL), sponsored by the National Science Foundation and other agencies. We would like to acknowledge high-performance computing support from Yellowstone (ark:/85065/d7wd3xhc) provided by NCAR's Computational and Information Systems Laboratory, sponsored by the National Science Foundation [*Computational and Information Systems Laboratory*, 2012]. The CESM project is supported by the National Science Foundation and the Office of Science (BER) of the U.S. Department of Energy. The NCAR MOPITT project is supported by NASA's Earth Observing System Program. The National Center for Atmospheric Research is sponsored by the National Science Foundation. Any opinions, findings, and conclusions or recommendations expressed in this publication are those of the author and do not necessarily reflect the views of the National Science Foundation. A.F.A. acknowledges NASA supports under grants NNX13AK24G and NNX14AN47G.

NCEP	National Centers for Environmental Prediction.
NDACC	Network for the Detection of Atmospheric Composition Change.
NMVOCs	nonmethane volatile organic compounds.
NOAA	National Oceanic and Atmospheric Administration.
POP	Parallel Ocean Program.
RMSE	root-mean-square error.
SMOCC	Smoke Aerosols, Clouds, Rainfall, and Climate.
TES	Tropospheric Emissions Spectrometer.
VOCs	volatile organic compounds.
WACCM	Whole Atmosphere Community Climate Model.
WDCGG	World Data Centre for Greenhouse Gases.

References

Anderson, J. L. (2001), An ensemble adjustment Kalman filter for data assimilation, *Mon. Weather Rev.*, *129*, 2884–2903.

Anderson, J. L. (2003), A local least squares framework for ensemble filtering, *Mon. Weather Rev.*, *131*, 634–642.

Anderson, J. L. (2009b), Spatially and temporally varying adaptive covariance inflation for ensemble filters, *Tellus A*, *61*, 72–83, doi:10.1111/j.1600-0870.2008.00361.x.

Anderson, J. L., T. Hoar, K. Raeder, H. Liu, N. Collins, R. Torn, and A. Avellino (2009a), The Data Assimilation Research Testbed: A community facility, *Bull. Am. Meteorol. Soc.*, *90*, 1283–1296.

Andreae, M. O., D. Rosenfeld, P. Artaxo, A. A. Costa, G. P. Frank, K. M. Longo, and M. A. F. Silvas-Dias (2004), Smoking rain clouds over the Amazon, *Science*, *303*, 1337–1342.

Andreae, M. O., P. Artaxo, V. Beck, M. Bela, C. Gerbig, K. Longo, J. W. Munger, K. T. Wiedemann, and S. C. Wofsy (2012), Carbon monoxide and related trace gases and aerosols over the Amazon Basin during the wet and dry seasons, *Atmos. Chem. Phys.*, *12*, 6041–6065.

Andreae, M., and P. Merlet (2001), Emission of trace gases and aerosols from biomass burning, *Global Biogeochem. Cycles*, *15*, 955–966, doi:10.1029/2000GB001382.

Arellano, A. F., Jr., P. S. Kasibhatla, L. Giglio, G. R. van der Werf, and J. T. Randerson (2004), Topdown estimates of global CO sources using MOPITT measurements, *Geophys. Res. Lett.*, *31*, L01104, doi:10.1029/2003GL018609.

Arellano, A. F., Jr., P. S. Kasibhatla, L. Giglio, G. R. van der Werf, J. T. Randerson, and G. J. Collatz (2006), Time-dependent inversion estimates of global biomass-burning CO emissions using Measurement of Pollution in the Troposphere (MOPITT) measurements, *J. Geophys. Res.*, *111*, D09303, doi:10.1029/2005JD006613.

Arellano, A. F., Jr., K. Raeder, J. L. Anderson, P. G. Hess, L. K. Emmons, D. P. Edwards, G. G. Pfister, T. L. Campos, and G. W. Sachse (2007), Evaluating model performance of an ensemble-based chemical data assimilation system during INTEX-B field mission, *Atmos. Chem. Phys.*, *7*, 5695–5710, doi:10.5194/acp-7-5695.

Arellano, A. F., Jr., P. G. Hess, D. P. Edwards, and D. Baumgardner (2010), Constraints on black carbon aerosol distribution from Measurements of Pollution in the Troposphere (MOPITT) CO, *Geophys. Res. Lett.*, *37*, L17801, doi:10.1029/2010GL044416.

Artaxo, P., L. V. Rizzo, J. F. Brito, H. M. J. Barbosa, A. Arana, E. T. Sena, G. G. Cirino, W. Bastos, S. T. Martin, and M. O. Andreae (2013), Atmospheric aerosols in Amazonia and land use change: From natural biogenic to biomass burning conditions, *Faraday Discuss.*, *165*, 203–235, doi:10.1039/C3FD00052D.

Baklanov, A., et al. (2014), Online coupled regional meteorology chemistry models in Europe: Current status and prospects, *Atmos. Chem. Phys.*, *14*, 317–398, doi:10.5194/acp-14-317-2014.

Barré, J., L. El Amraoui, P. Ricaud, W. A. Lahoz, J.-L. Attié, V.-H. Peuch, B. Josse, and V. Marécal (2013), Diagnosing the transition layer at extratropical latitudes using MLS O_3 and MOPITT CO analyses, *Atmos. Chem. Phys.*, *13*, 7225–7240, doi:10.5194/acp-13-7225-2013.

Barré, J., et al. (2015), Assessing the impacts of assimilating IASI and MOPITT CO retrievals using CESM-CAM-chem and DART, *J. Geophys. Res. Atmos.*, *120*, 10,501–10,529, doi:10.1002/2015JD023467.

Bocquet, M., and P. Sakov (2014), An iterative ensemble Kalman smoother, *Q. J. R. Meteorol. Soc.*, *140*, 1521–1535, doi:10.1002/qj.2236.

Butler, T. M., P. J. Rayner, I. Simmonds, and M. G. Lawrence (2005), Simultaneous mass balance inverse modeling of methane and carbon monoxide, *J. Geophys. Res.*, *110*, D21310, doi:10.1029/2005JD006071.

Chevallier, F., A. Fortems, P. Bousquet, I. Pison, S. Szopa, M. Devaux, and D. A. Hauglustaine (2009), African CO emissions between years 2000 and 2006 as estimated from MOPITT observations, *Biogeosciences*, *6*, 103–111, doi:10.5194/bg-6-103-2009.

Clerbaux, C., et al. (2015), Tracking pollutants from space: Eight years of IASI satellite observation, *C. R. Geosci.*, *347*(3), 134–144.

Coman, A., G. Foret, M. Beekmann, M. Eremenko, G. Dufour, B. Gaubert, A. Ung, C. Schmechtig, J.-M. Flaud, and G. Bergametti (2012), Assimilation of IASI partial tropospheric columns with an Ensemble Kalman Filter over Europe, *Atmos. Chem. Phys.*, *12*, 2513–2532, doi:10.5194/acp-12-2513-2012.

Computational and Information Systems Laboratory (2012), *Yellowstone: IBM iDataPlex System (NCAR Community Computing)*, Natl. Cent. for Atmos. Res., Boulder, Colo. [Available at http://n2t.net/ark:/85065/d7wd3xhc.]

Constantinescu, E. M., A. Sandu, T. Chai, and G. Carmichael (2007a), Ensemble-based chemical data assimilation. I: General approach, *Q. J. R. Meteorol. Soc.*, *133*, 1229–1243, doi:10.1002/qj.76.

Constantinescu, E. M., A. Sandu, T. Chai, and G. R. Carmichael (2007b), Ensemble-based chemical data assimilation. II: Covariance localization, *Q. J. R. Meteorol. Soc.*, *133*, 1245–1256.

Crutzen, P. J. (1973), A discussion of the chemistry of some minor constituents in the stratosphere and troposphere, *Pure App. Geophys.*, *106*, 1385–1399.

Curier, R. L., R. Timmermans, S. Calabretta-Jongen, H. Eskes, A. Segers, D. Swart, and M. Schaap (2012), Improving ozone forecasts over Europe by synergistic use of the LOTOS-EUROS chemical transport model and in-situ measurements, *Atmos. Environ.*, *60*, 217–226.

Daskalakis, N., S. Myriokefalitakis, and M. Kanakidou (2015), Sensitivity of tropospheric loads and lifetimes of short lived pollutants to fire emissions, *Atmos. Chem. Phys.*, *15*, 3543–3563, doi:10.5194/acp-15-3543-2015.

De Smedt, I., et al. (2015), Diurnal, seasonal and long-term variations of global formaldehyde columns inferred from combined OMI and GOME-2 observations, *Atmos. Chem. Phys.*, *15*, 12,519–12,545, doi:10.5194/acp-15-12519-2015.

Deeter, M. N., S. Martínez-Alonso, D. P. Edwards, L. K. Emmons, J. C. Gille, H. M. Worden, J0. V. Pittman, B. C. Daube, and S. C. Wofsy (2013), Validation of MOPITT Version 5 thermal-infrared, near-infrared, and multispectral carbon monoxide profile retrievals for 2000–2011, *J. Geophys. Res. Atmos.*, *118*, 6710–6725, doi:10.1002/jgrd.50272.

Deeter, M. N., S. Martínez-Alonso, D. P. Edwards, L. K. Emmons, J. C. Gille, H. M. Worden, C. Sweeney, J. V. Pittman, B. C. Daube, and S. C. Wofsy (2014), The MOPITT Version 6 product: Algorithm enhancements and validation, *Atmos. Meas. Tech.*, *7*, 3623–3632, doi:10.5194/amt-7-3623-2014.

Duncan, B. N., R. V. Martin, A. C. Staudt, R. Yevich, and J. A. Logan (2003), Interannual and seasonal variability of biomass burning emissions constrained by satellite observations, *J. Geophys. Res.*, *108*(D2), 4100, doi:10.1029/2002JD002378.

Duncan, B. N., J. A. Logan, I. Bey, I. A. Megretskaia, R. M. Yantosca, P. C. Novelli, N. B. Jones, and C. P. Rinsland (2007), Global budget of CO, 1988–1997: Source estimates and validation with a global model, *J. Geophys. Res.*, *112*, D22301, doi:10.1029/2007JD008459.

Edwards, D. P., C. Halvorson, and J. C. Gille (1999), Radiative transfer modeling for the EOS Terra satellite Measurement of Pollution in the Troposphere (MOPITT) instrument, *J. Geophys. Res.*, *104*, 16,755–16,775.

Edwards, D. P., et al. (2004), Observations of carbon monoxide and aerosols from the Terra satellite: Northern Hemisphere variability, *J. Geophys. Res.*, *109*, D24202, doi:10.1029/2004JD004727.

Edwards, D. P., G. Pétron, P. C. Novelli, L. K. Emmons, J. C. Gille, and J. R. Drummond (2006a), Southern Hemisphere carbon monoxide interannual variability observed by Terra/Measurement of Pollution in the Troposphere (MOPITT), *J. Geophys. Res.*, *111*, D16303, doi:10.1029/2006JD007079.

Edwards, D. P., et al. (2006b), Satellite-observed pollution from Southern Hemisphere biomass burning, *J. Geophys. Res.*, *111*, D14312, doi:10.1029/2005JD006655.

Emmons, L. K., et al. (2004), Validation of Measurements of Pollution in the Troposphere (MOPITT) CO retrievals with aircraft in situ profiles, *J. Geophys. Res.*, *109*, D03309, doi:10.1029/2003JD004101.

Emmons, L. K., et al. (2010), Description and evaluation of the Model for Ozone and Related chemical Tracers, version 4 (MOZART-4), *Geosci. Model Dev.*, *3*, 43–67, doi:10.5194/gmd-3-43-2010.

Emmons, L. K., et al. (2015), The POLARCAT Model Intercomparison Project (POLMIP): Overview and evaluation with observations, *Atmos. Chem. Phys.*, *15*, 6721–6744, doi:10.5194/acp-15-6721-2015.

Evensen, G. (2003), The ensemble Kalman filter: Theoretical formulation and practical implementation, *Ocean Dynam.*, *53*, 343–367.

Fortems-Cheiney, A., F. Chevallier, I. Pison, P. Bousquet, C. Carouge, C. Clerbaux, P.-F. Coheur, M. George, D. Hurtmans, and S. Szopa (2009), On the capability of IASI measurements to inform about CO surface emissions, *Atmos. Chem. Phys.*, *9*, 8735–8743, doi:10.5194/acp-9-8735-2009.

Fortems-Cheiney, A., F. Chevallier, I. Pison, P. Bousquet, S. Szopa, M. N. Deeter, and C. Clerbaux (2011), Ten years of CO emissions as seen from Measurements of Pollution in the Troposphere (MOPITT), *J. Geophys. Res.*, *116*, D05304, doi:10.1029/2010JD014416.

Fortems-Cheiney, A., F. Chevallier, I. Pison, P. Bousquet, M. Saunois, S. Szopa, C. Cressot, T. P. Kurosu, K. Chance, and A. Fried (2012), The formaldehyde budget as seen by a global-scale multi-constraint and multi-species inversion system, *Atmos. Chem. Phys.*, *12*(15), 6699–6721, doi:10.5194/acp-12-6699-2012.

Freitas, S. R., K. M. Longo, and M. O. Andreae (2006), Impact of including the plume rise of vegetation fires in numerical simulations of associated atmospheric pollutants, *Geophys. Res. Lett.*, *33*, L17808, doi:10.1029/2006GL026608.

Freitas, S. R., K. M. Longo, R. Chatfield, D. Latham, M. A. F. Silva Dias, M. O. Andreae, E. Prins, J. C. Santos, R. Gielow, and J. A. Carvalho Jr. (2007), Including the sub-grid scale plume rise of vegetation fires in low resolution atmospheric transport models, *Atmos. Chem. Phys.*, *7*, 3385–3398, doi:10.5194/acp-7-3385-2007.

Fuzzi, S., et al. (2007), Overview of the inorganic and organic composition of size-segregated aerosol in Rondonia, Brazil, from the biomass-burning period to the onset of the wet season, *J. Geophys. Res.*, *112*, D01201, doi:10.1029/2005JD006741.

Gaspari, G., and S. E. Cohn (1999), Construction of correlation functions in two and three dimensions, *Q. J. R. Meteorol. Soc.*, *125*, 723–757.

Gaubert, B., A. Coman, G. Foret, F. Meleux, A. Ung, L. Rouil, A. Ionescu, Y. Candau, and M. Beekmann (2014), Regional scale ozone data assimilation using an ensemble Kalman filter and the CHIMERE chemical transport model, *Geosci. Model Dev.*, *7*, 283–302, doi:10.5194/gmd-7-283-2014.

George, M., et al. (2015), An examination of the long-term CO records from MOPITT and IASI comparison of retrieval methodology, *Atmos. Meas. Tech.*, *8*, 4313–4328, doi:10.5194/amt-8-4313-2015.

Granier, C., G. Pétron, J.-F. Muller, and G. Brasseur (2000), The impact of natural and anthropogenic hydrocarbons on the tropospheric budget of carbon monoxide, *Atmos. Environ.*, *34*, 5255–5270.

Granier, C., et al. (2011), Evolution of anthropogenic and biomass burning emissions of air pollutants at global and regional scales during the 1980–2010 period, *Clim. Change*, *109*, 163–190, doi:10.1007/s10584-011-0154-1.

Guenther, A. B., X. Jiang, C. L. Heald, T. Sakulyanontvittaya, T. Duhl, L. K. Emmons, and X. Wang (2012), The Model of Emissions of Gases and Aerosols from Nature version 2.1 (MEGAN2.1): An extended and updated framework for modeling biogenic emissions, *Geosci. Model Dev.*, *5*, 1471–1492, doi:10.5194/gmd-5-1471-2012.

Gurney, K. R., et al. (2002), Towards robust regional estimates of CO_2 sources and sinks using atmospheric transport models, *Nature*, *415*, 626–630.

Guthrie, P. (1989), The CH4-CO-OH conundrum: A simple analytic approach, *Global Biogeochem. Cycles*, *4*, 287–298, doi:10.1029/GB003i004p00287.

Guyon, P., et al. (2005), Airborne measurements of trace gases and aerosol particle emissions from biomass burning in Amazonia, *Atmos. Chem. Phys.*, *5*, 2989–3002.

Hanea, R. G., G. J. M. Velders, and A. Heemink (2004), Data assimilation of ground-level ozone in Europe with a Kalman filter and chemistry transport model, *J. Geophys. Res.*, *109*, D10302, doi:10.1029/2003JD004283.

Hannigan, J., M. T. Coffey, and A. Goldman (2009), Semiautonomous FTS observation system for remote sensing of stratospheric and tropospheric gases, *J. Atmos. Oceanic Technol.*, *26*, 1814–1828.

Heald, C. L., D. J. Jacob, D. B. A. Jones, P. I. Palmer, J. A. Logan, D. G. Streets, G. W. Sachse, J. C. Gille, R. N. Hoffman, and T. Nehrkorn (2004), Comparative inverse analysis of satellite (MOPITT) and aircraft (TRACE-P) observations to estimate Asian sources of carbon monoxide, *J. Geophys. Res.*, *109*, D15S04, doi:10.1029/2004JD005185.

Hodzic, A., and J. L. Jimenez (2011), Modeling anthropogenically controlled secondary organic aerosols in a megacity: A simplified framework for global and climate models, *Geosci. Model Dev.*, *4*, 901–917, doi:10.5194/gmd-4-901-2011.

Hooghiemstra, P. B., M. C. Krol, P. Bergamaschi, A. T. J. de Laat, G. R. van der Werf, P. C. Novelli, M. N. Deeter, I. Aben, and T. Rockmann (2012), Comparing optimized CO emission estimates using MOPITT or NOAA surface network observations, *J. Geophys. Res.*, *117*, D06309, doi:10.1029/2011JD017043.

Hudman, R. C., L. T. Murray, D. J. Jacob, D. B. Millet, S. Turquety, S. Wu, D. R. Blake, A. H. Goldstein, J. Holloway, and G. W. Sachse (2008), Biogenic versus anthropogenic sources of CO in the United States, *Geophys. Res. Lett.*, *35*, L04801, doi:10.1029/2007GL032393.

Hunke, E. C., and W. H. Lipscomb (2008), CICE: The Los Alamos Sea Ice Model, Documentation and Software, Version 4.0, Los Alamos Natl. Lab. Tech. Rep. LA-CC-06-012.

Hurrell, J. W., et al. (2013), The Community Earth System Model: A framework for collaborative research, *Bull. Am. Meteorol. Soc.*, *94*, 1339–1360.

Inness, A., et al. (2013), The MACC reanalysis: An 8 yr data set of atmospheric composition, *Atmos. Chem. Phys.*, *13*, 4073–4109, doi:10.5194/acp-13-4073-2013.

Inness, A., et al. (2015), Data assimilation of satellite retrieved ozone, carbon monoxide and nitrogen dioxide with ECMWF's Composition-IFS, *Atmos. Chem. Phys.*, *15*, 5275–5303, doi:10.5194/acp-15-5275-2015.

Isaksen, I. S. A., et al. (2009), Atmospheric composition change: Climate-Chemistry interactions, *Atmos. Environ.*, *43*, 5138–5192, doi:10.1016/j.atmosenv.2009.08.003.

Jiang, Z., D. B. A. Jones, M. Kopacz, J. Liu, D. K. Henze, and C. Heald (2011), Quantifying the impact of model errors on top-down estimates of carbon monoxide emissions using satellite observations, *J. Geophys. Res.*, *116*, D15306, doi:10.1029/2010JD015282.

Jiang, Z., D. B. A. Jones, H. M. Worden, M. N. Deeter, D. K. Henze, J. Worden, K. W. Bowman, C. A. M. Brenninkmeijer, and T. J. Schuck (2013), Impact of model errors in convective transport on CO source estimates inferred from MOPITT CO retrievals, *J. Geophys. Res. Atmos.*, *118*, 2073–2083, doi:10.1002/jgrd.50216.

Jiang, Z., D. B. A. Jones, H. M. Worden, and D. K. Henze (2015), Sensitivity of top-down CO source estimates to the modeled vertical structure in atmospheric CO, *Atmos. Chem. Phys.*, *15*, 1521–1537, doi:10.5194/acp-15-1521-2015.

Jones, D. B. A., K. W. Bowman, P. I. Palmer, J. R. Worden, D. J. Jacob, R. N. Hoffman, I. Bey, and R. M. Yantosca (2003), Potential of observations from the Tropospheric Emission Spectrometer to constrain continental sources of carbon monoxide, *J. Geophys. Res.*, *108*(D24), 4789, doi:10.1029/2003JD003702.

Jones, D. B. A., K. W. Bowman, J. A. Logan, C. L. Heald, J. Liu, M. Luo, J. Worden, and J. Drummond (2009), The zonal structure of tropical O_3 and CO as observed by the Tropospheric Emission Spectrometer in November 2004—Part 1: Inverse modeling of CO emissions, *Atmos. Chem. Phys.*, *9*, 3547–3562, doi:10.5194/acp-9-3547-2009.

Jones, N. B., C. P. Rinsland, J. B. Liley, and J. Rosen (2001), Correlation of aerosol and carbon monoxide at 45°S: Evidence of biomass burning emissions, *Geophys. Res. Lett.*, *28*, 709–712, doi:10.1029/2000GL012203.

Kaiser, J. W., et al. (2012), Biomass burning emissions estimated with a global fire assimilation system based on observed fire radiative power, *Biogeosciences*, *9*, 527–554, doi:10.5194/bg-9-527-2012.

Kang, J. S., E. Kalnay, J. Liu, I. Fung, T. Miyoshi, and K. Ide (2011), "Variable localization" in an ensemble Kalman filter: Application to the carbon cycle data assimilation, *J. Geophys. Res.*, *116*, D09110, doi:10.1029/2010JD014673.

Khattatov, B. V., P. G. Hess, L. V. Lyjak, J. C. Gille, D. P. Edwards, M. N. Deeter, and L. K. Emmons (2004), Assimilation of the 2000–2001 CO MOPITT retrievals with optimized surface emissions, *Geophys. Res. Lett.*, *31*, L20105, doi:10.1029/2004GL021037.

Klonecki, A., et al. (2012), Assimilation of IASI satellite CO fields into a global chemistry transport model for validation against aircraft measurements, *Atmos. Chem. Phys.*, *12*, 4493–4512, doi:10.5194/acp-12-4493-2012.

Kondo, Y., et al. (2011), Emissions of black carbon, organic, and inorganic aerosols from biomass burning in North America and Asia in 2008, *J. Geophys. Res.*, *116*, D08204, doi:10.1029/2010JD015152.

Konovalov, I. B., M. Beekmann, I. N. Kuznetsova, A. Yurova, and A. M. Zvyagintsev (2011), Atmospheric impacts of the 2010 Russian wildfires: Integrating modelling and measurements of an extreme air pollution episode in the Moscow region, *Atmos. Chem. Phys.*, *11*, 10,031–10,056, doi:10.5194/acp-11-10031-2011.

Kopacz, M., D. J. Jacob, D. K. Henze, C. L. Heald, D. G. Streets, and Q. Zhang (2009), Comparison of adjoint and analytical Bayesian inversion methods for constraining Asian sources of carbon monoxide using satellite (MOPITT) measurements of CO columns, *J. Geophys. Res.*, *114*, D04305, doi:10.1029/2007JD009264.

Kopacz, M., et al. (2010), Global estimates of CO sources with high resolution by adjoint inversion of multiple satellite datasets (MOPITT, AIRS, SCIAMACHY, TES), *Atmos. Chem. Phys.*, *10*, 855–876, doi:10.5194/acp-10-855-2010.

Krol, M., et al. (2013), How much CO was emitted by the 2010 fires around Moscow?, *Atmos. Chem. Phys.*, *13*, 4737–4747, doi:10.5194/acp-13-4737-2013.

Lamarque, J. F., et al. (2010), Historical (1850–2000) gridded anthropogenic and biomass burning emissions of reactive gases and aerosols: Methodology and application, *Atmos. Chem. Phys.*, *10*(15), 7017–7039, doi:10.5194/acp-10-7017-2010.

Lamarque, J.-F., et al. (2004), Application of a bias estimator for the improved assimilation of Measurements of Pollution in the Troposphere (MOPITT) carbon monoxide retrievals, *J. Geophys. Res.*, *109*, D16304, doi:10.1029/2003JD004466.

Lamarque, J.-F., et al. (2012), CAM-chem: Description and evaluation of interactive atmospheric chemistry in the Community Earth System Model, *Geosci. Model Dev.*, *5*, 369–411, doi:10.5194/gmd-5-369-2012.

Lawrence, D., et al. (2011), Parameterization improvements and functional structural advances in version 4 of the Community Land Model, *J. Adv. Model. Earth Syst.*, *3*, 03001, doi:10.1029/2011MS000045.

Lelieveld, J., S. Gromov, A. Pozzer, and D. Taraborrelli (2016), Global tropospheric hydroxyl distribution, budget and reactivity, *Atmos. Chem. Phys. Discuss.*, doi:10.5194/acp-2016-160, in review.

Levy, H. (1971), Normal atmosphere: Large radical and formaldehyde concentrations predicted, *Science*, *173*, 141–143.

Liu, J., I. Fung, E. Kalnay, and J.-S. Kang (2011), CO_2 transport uncertainties from the uncertainties in meteorological fields, *Geophys. Res. Lett.*, *38*, L12808, doi:10.1029/2011GL047213.

Logan, J. A., M. J. Prather, S. C. Wofsy, and M. B. McElroy (1981), Tropospheric chemistry: A global perspective, *J. Geophys. Res.*, *86*, 7210–7254, doi:10.1029/JC086iC08p07210.

Logan, J. A., I. A. Megretskaia, R. Nassar, L. T. Murray, L. Zhang, K. W. Bowman, H. M. Worden, and M. Luo (2008), Effects of the 2006 El Nino on tropospheric composition as revealed by data from the Tropospheric Emission Spectrometer (TES), *Geophys. Res. Lett.*, *35*, L03816, doi:10.1029/2007GL031698.

Mao, J., S. Fan, D. J. Jacob, and K. R. Travis (2013), Radical loss in the atmosphere from Cu-Fe redox coupling in aerosols, *Atmos. Chem. Phys.*, *13*, 509–519, doi:10.5194/acp-13-509-2013.

Marais, E. A., et al. (2012), Isoprene emissions in Africa inferred from OMI observations of formaldehyde columns, *Atmos. Chem. Phys.*, *12*, 6219–6235, doi:10.5194/acp-12-6219-2012.

Marenco, A., et al. (1998), Measurement of ozone and water vapor by Airbus in-service aircraft: The MOZAIC airborne program—An overview, *J. Geophys. Res.*, *103*, 25,631–25,642, doi:10.1029/98JD00977.

Marsh, D. R., M. J. Mills, D. E. Kinnison, J.-F. Lamarque, N. Calvo, and L. M. Polvani (2013), Climate change from 1850 to 2005 simulated in CESM1 (WACCM), *J. Clim.*, *26*, 7372–7391, doi:10.1175/JCLI-D-12-00558.1.

Ménard, R., and L.-P. Chang (2000), Assimilation of stratospheric chemical tracer observations using a Kalman filter. Part II: Chi-2-validated results and analysis of variance and correlation dynamics, *Mon. Weather Rev.*, *128*, 2672–2686.

Miyazaki, K., H. J. Eskes, K. Sudo, M. Takigawa, M. van Weele, and K. F. Boersma (2012b), Simultaneous assimilation of satellite NO_2, O_3, CO, and HNO_3 data for the analysis of tropospheric chemical composition and emissions, *Atmos. Chem. Phys.*, *12*, 9545–9579, doi:10.5194/acp-12-9545-2012.

Miyazaki, K., H. J. Eskes, and K. Sudo (2015), A tropospheric chemistry reanalysis for the years 2005–2012 based on an assimilation of OMI, MLS, TES, and MOPITT satellite data, *Atmos. Chem. Phys.*, *15*, 8315–8348, doi:10.5194/acp-15-8315-2015.

Monks, S. A., et al. (2015), Multi-model study of chemical and physical controls on transport of anthropogenic and biomass burning pollution to the Arctic, *Atmos. Chem. Phys.*, *15*, 3575–3603, doi:10.5194/acp-15-3575-2015.

Montzka, S., M. Krol, E. Dlugokencky, B. Hall, P. Jöckel, and J. Lelieveld (2011), Small inter-annual variability of global atmospheric hydroxyl, *Science*, *331*, 67–69.

Morgenstern, O., G. Zeng, S. W. Wood, J. Robinson, D. Smale, C. Paton-Walsh, N. B. Jones, and D. W. T. Griffith (2012), Long-range correlations in Fourier transform infrared, satellite, and modeled CO in the Southern Hemisphere, *J. Geophys. Res.*, *117*, D11301, doi:10.1029/2012JD017639.

Muller, J.-F., and T. Stavrakou (2005), Inversion of CO and NO_x emissions using the adjoint of the IMAGES model, *Atmos. Chem. Phys.*, *5*, 1157–1186, doi:10.5194/acp-5-1157-2005.

Naik, V., et al. (2013), Preindustrial to present-day changes in tropospheric hydroxyl radical and methane lifetime from the Atmospheric Chemistry and Climate Model Intercomparison Project (ACCMIP), *Atmos. Chem. Phys.*, *13*, 5277–5298, doi:10.5194/acp-13-5277-2013.

Neale, R., J. Richter, S. Park, P. H. Lauritzen, S. J. Vavrus, P. J. Rasch, and M. Zhang (2013), The mean climate of the Community Atmosphere Model (CAM4) in forced SST and fully coupled experiments, *J. Clim.*, *26*, 5150–5168.

Nédélec, P., J.-P. Cammas, V. Thouret, G. Athier, J.-M. Cousin, C. Legrand, C. Abonnel, F. Lecoeur, G. Cayez, and C. Marizy (2003), An improved infrared carbon monoxide analyser for routine measurements aboard commercial Airbus aircraft: Technical validation and first scientific results of the MOZAIC III programme, *Atmos. Chem. Phys.*, *3*, 1551–1564.

Notholt, J., R. Neuber, O. Schrems, and T. von Clarmann (1993), Stratospheric trace gas concentrations in the Arctic polar night derived by FTIR-spectroscopy with the moon as IR light source, *Geophys. Res. Lett.*, *20*, 2059–2062, doi:10.1029/93GL01971.

Notholt, J., G. C. Toon, F. Stordal, S. Solberg, N. Schmidbauer, A. Meier, E. Becker, and B. Sen (1997), Seasonal variations of atmospheric trace gases in the high Arctic at 79°N, *J. Geophys. Res.*, *102*, 12,855–12,861, doi:10.1029/97JD00337.

Novelli, P. C., and K. A. Masarie (2015), Atmospheric Carbon Monoxide Dry Air Mole Fractions from the NOAA ESRL Carbon Cycle Cooperative Global Air Sampling Network, 1988–2014, Version: 2015-08-04. [Available at ftp://aftp.cmdl.noaa.gov/data/trace_gases/co/flask/surface/.]

Novelli, P. C., K. A. Masarie, and P. M. Lang (1998), Distributions and recent changes in carbon monoxide in the lower troposphere, *J. Geophys. Res.*, *103*, 19,015–19,033, doi:10.1029/98JD01366.

Novelli, P. C., K. A. Masarie, P. M. Lang, B. D. Hall, R. C. Myers, and J. W. Elkins (2003), Reanalysis of tropospheric CO trends: Effects of the 1997–1998 wildfires, *J. Geophys. Res.*, *108*(D15), 4464, doi:10.1029/2002JD003031.

Pagowski, M., and G. A. Grell (2012), Experiments with the assimilation of fine aerosols using an ensemble Kalman filter, *J. Geophys. Res.*, *117*, D21302, doi:10.1029/2012JD018333.

Palmer, P. I., D. J. Jacob, D. B. A. Jones, C. L. Heald, R. M. Yantosca, J. A. Logan, G. W. Sachse, and D. G. Streets (2003), Inverting for emissions of carbon monoxide from Asia using aircraft observations over the western Pacific, *J. Geophys. Res.*, *108*(D21), 4180, doi:10.1029/2003JD003397.

Paton-Walsh, C., N. B. Jones, S. R. Wilson, V. Haverd, A. Meier, D. W. T. Griffith, and C. P. Rinsland (2005), Measurements of trace gas emissions from Australian forest fires and correlations with coincident measurements of aerosol optical depth, *J. Geophys. Res.*, *110*, D24305, doi:10.1029/2005JD006202.

Patra, P. K., et al. (2011), TransCom model simulations of CH_4 and related species: Linking transport, surface flux and chemical loss with CH_4 variability in the troposphere and lower stratosphere, *Atmos. Chem. Phys.*, *11*, 12,813–12,837, doi:10.5194/acp-11-12813-2011.

Patra, P. K., et al. (2014), Observational evidence for interhemispheric hydroxyl parity, *Nature*, *513*, 219–223.

Pétron, G., C. Granier, B. Khattatov, V. Yudin, J. F. Lamarque, L. Emmons, J. Gille, and D. P. Edwards (2004), Monthly CO surface sources inventory based on the 2000–2001 MOPITT satellite data, *Geophys. Res. Lett.*, *31*, L21107, doi:10.1029/2004GL020560.

Pfister, G., P. G. Hess, L. K. Emmons, J.-F. Lamarque, C. Wiedinmyer, D. P. Edwards, G. Pétron, J. C. Gille, and G. W. Sachse (2005), Quantifying CO emissions from the 2004 Alaskan wildfires using MOPITT CO data, *Geophys. Res. Lett.*, *32*, L11809, doi:10.1029/2005GL022995.

Pison, I., P. Bousquet, F. Chevallier, S. Szopa, and D. Hauglustaine (2009), Multi-species inversion of CH_4, CO and H_2 emissions from surface measurements, *Atmos. Chem. Phys.*, *9*, 5281–5297, doi:10.5194/acp-9-5281-2009.

Pradier, S., J.-L. Attie, M. Chong, J. Escobar, V.-H. Peuch, J.-F. Lamarque, B. Kattatov, and D. Edwards (2006), Evaluation of 2001 springtime CO transport over West Africa using MOPITT CO measurements assimilated in a global chemistry transport model, *Tellus*, *58B*, 163–176.

Prather, M. J. (1996), Time scale in atmospheric chemistry: Theory, GWPs for CH_4 and CO, and runaway growth, *Geophys. Res. Lett.*, *23*, 2597–2600, doi:10.1029/96GL02371.

Prather, M. J., C. D. Holmes, and J. Hsu (2012), Reactive greenhouse gas scenarios: Systematic exploration of uncertainties and the role of atmospheric chemistry, *Geophys. Res. Lett.*, *39*, L09803, doi:10.1029/2012GL051440.

Prather, M., et al. (2001), Atmospheric chemistry and greenhouse gases, in *Climate Change 2001*, edited by J. T. Houghton, pp. 239–287, Cambridge Univ. Press, New York.

Prinn, R. G. (2005), Evidence for variability of atmospheric hydroxyl radicals over the past quarter century, *Geophys. Res. Lett.*, *32*, L07809, doi:10.1029/2004GL022228.

Raeder, K., J. L. Anderson, N. Collins, T. J. Hoar, J. E. Kay, P. H. Lauritzen, and R. Pincus (2012), DART/CAM: An ensemble data assimilation system for CESM atmospheric models, *J. Clim.*, *25*, 6304–6317, doi:10.1175/JCLI-D-11-00395.1.

Rayner, N. A., P. Brohan, D. E. Parker, C. K. Folland, J. J. Kennedy, M. Vanicek, T. J. Ansell, and S. F. B. Tett (2006), Improved analyses of changes and uncertainties in sea surface temperature measured in situ since the mid-nineteenth century: The HadSST2 dataset, *J. Clim.*, *19*, 446–469.

Seinfeld, J. H., and S. N. Pandis (1998), *Atmospheric Chemistry and Physics: From Air Pollution to Climate Change*, John Wiley, New York.

Shindell, D. T., et al. (2006), Multimodel simulations of carbon monoxide: Comparison with observations and projected near-future changes, *J. Geophys. Res.*, *111*, D19306, doi:10.1029/2006JD007100.

Silva, S. J., A. F. Arellano, and H. Worden (2013), Toward anthropogenic combustion emission constraints from space-based analysis of urban CO_2/CO sensitivity, *Geophys. Res. Lett.*, *40*, 4971–4976, doi:10.1002/grl.50954.

Smith, R., et al. (2010), The Parallel Ocean Program (POP) reference manual, Ocean Component of the Community Climate System Model (CCSM) and Community Earth System Model (CESM), Los Alamos Natl. Lab. Tech. Rep. LAUR-10-01853.

Song, X., L. Shi, M. Ye, J. Yang, and I. M. Navon (2014), Numerical comparison of iterative ensemble Kalman filters for unsaturated flow inverse modeling, *Vadose Zone J*, *13*(2), 1–12, doi:10.2136/vzj2013.05.0083.

Stavrakou, T., and J. F. Muller (2006), Grid-based versus big region approach for inverting CO emissions using Measurement of Pollution in the Troposphere (MOPITT) data, *J. Geophys. Res.*, *111*, D15304, doi:10.1029/2005JD006896.

Stein, O., M. G. Schultz, I. Bouarar, H. Clark, V. Huijnen, A. Gaudel, M. George, and C. Clerbaux (2014), On the wintertime low bias of Northern Hemisphere carbon monoxide found in global model simulations, *Atmos. Chem. Phys.*, *14*, 9295–9316, doi:10.5194/acp-14-9295-.

Stocker, T. F., et al. (2013), Technical summary, in *Climate Change 2013: The Physical Sciences Basis, Contribution of Working Group I to the Fifth Assessment Report of the Intergovernmental Panel on Climate Change*, 1535 pp., Cambridge Univ. Press, Cambridge, U. K., and New York, doi:10.1017/CBO9781107415324.

Streets, D. G., et al. (2013), Emissions estimation from satellite retrievals: A review of current capability, *Atmos. Environ.*, *77*, 1011–1042, doi:10.1016/j.atmosenv.2013.05.051.

Strode, S. A., B. N. Duncan, E. A. Yegorova, J. Kouatchou, J. R. Ziemke, and A. R. Douglass (2015), Implications of carbon monoxide bias for methane lifetime and atmospheric composition in chemistry climate models, *Atmos. Chem. Phys.*, *15*, 11,789–11,805, doi:10.5194/acp-15-11789-2015.

Tang, X., J. Zhu, Z. F. Wang, and A. Gbaguidi (2011), Improvement of ozone forecast over Beijing based on ensemble Kalman filter with simultaneous adjustment of initial conditions and emissions, *Atmos. Chem. Phys.*, *11*, 12901–12916.

Thonat, T., C. Crevoisier, N. A. Scott, A. Chédin, R. Armante, and L. Crépeau (2015), Signature of tropical fires in the diurnal cycle of tropospheric CO as seen from Metop-A/IASI, *Atmos. Chem. Phys.*, *15*, 13,041–13,057, doi:10.5194/acp-15-13041-2015.

Thouret, V., J.-P. Cammas, B. Sauvage, G. Athier, R. Zbinden, P. Nédélec, P. Simon, and F. Karcher (2006), Tropopause referenced ozone climatology and inter-annual variability (1994–2003) from the MOZAIC programme, *Atmos. Chem. Phys.*, *6*, 1033–1051, doi:10.5194/acp-6-1033-2006.

Tilmes, S., et al. (2015), Description and evaluation of tropospheric chemistry and aerosols in the Community Earth System Model (CESM1.2), *Geosci. Model Dev.*, *8*, 1395–1426, doi:10.5194/gmd-8-1395-2015.

Val Martin, M., J. A. Logan, R. A. Kahn, F.-Y. Leung, D. L. Nelson, and D. J. Diner (2010), Smoke injection heights from fires in North America: Analysis of 5 years of satellite observations, *Atmos. Chem. Phys.*, *10*, 1491–1510, doi:10.5194/acp-10-1491-2010.

Val Martin, M., C. L. Heald, and S. R. Arnold (2014), Coupling dry deposition to vegetation phenology in the Community Earth System Model: Implications for the simulation of surface O_3, *Geophys. Res. Lett.*, *41*, 2988–2996, doi:10.1002/2014GL059651.

Van der Werf, G. R., J. T. Randerson, L. Giglio, G. J. Collatz, P. S. Kasibhatla, and A. F. Arellano Jr. (2006), Interannual variability in global biomass burning emissions from 1997 to 2004, *Atmos. Chem. Phys.*, *6*, 3423–3441, doi:10.5194/acp-6-3423-2006.

Warner, J., M. M. Comer, C. D. Barnet, W. W. McMillan, W. Wolf, E. Maddy, and G. Sachse (2007), A comparison of satellite tropospheric carbon monoxide measurements from AIRS and MOPITT during INTEX-A, *J. Geophys. Res.*, *112*, D12S17, doi:10.1029/2006JD007925.

Whaley, C. H., et al. (2015), Toronto area ozone: Long-term measurements and modeled sources of poor air quality events, *J. Geophys. Res. Atmos.*, *120*, 11,368–11,390, doi:10.1002/2014JD022984.

Wiacek, A., J. R. Taylor, K. Strong, R. Saari, and T. E. Kerzenmacher (2007), Ground-based solar absorption FTIR spectroscopy: Characterization of retrievals and first results from a novel optical design instrument at a new NDACC complementary station, *J. Atmos. Oceanic Technol.*, *24*, 432–448, doi:10.1175/JTRCH1962.1.

Wiedinmyer, C., S. K. Akagi, R. J. Yokelson, L. K. Emmons, J. A. Al-Saadi, J. J. Orlando, and A. J. Soja (2011), The Fire INventory from NCAR (FINN): A high resolution global model to estimate the emissions from open burning, *Geosci. Model Dev.*, *4*, 625–641, doi:10.5194/gmd-4-625-2011.

Worden, H. M., M. N. Deeter, D. P. Edwards, J. C. Gille, J. R. Drummond, and P. Nédélec (2010), Observations of near surface carbon monoxide from space using MOPITT multispectral retrievals, *J. Geophys. Res.*, *115*, D18314, doi:10.1029/2010JD014242.

Worden, H. M., et al. (2013), Decadal record of satellite carbon monoxide observations, *Atmos. Chem. Phys.*, *13*, 837–850, doi:10.5194/acp-13-837-2013.

Worden, H. M., M. N. Deeter, D. P. Edwards, J. Gille, J. Drummond, L. K. Emmons, G. Francis, and S. Martínez-Alonso (2014), 13 years of MOPITT operations: Lessons from MOPITT retrieval algorithm development, *Ann. Geophys.*, *56*, doi:10.4401/ag-6330.

Wu, L., V. Mallet, M. Bocquet, and B. Sportisse (2008), A comparison study of data assimilation algorithms for ozone forecasts, *J. Geophys. Res.*, *113*, D20310, doi:10.1029/2008JD009991.

Yin, Y., F. Chevallier, P. Ciais, G. Broquet, A. Fortems-Cheiney, I. Pison, and M. Saunois (2015), Decadal trends in global CO emissions as seen by MOPITT, *Atmos. Chem. Phys.*, *15*, 13,433–13,451, doi:10.5194/acp-15-13433-2015.

Yudin, V. A., G. Pétron, J.-F. Lamarque, B. V. Khattatov, P. G. Hess, L. V. Lyjak, J. C. Gille, D. P. Edwards, M. N. Deeter, and L. K. Emmons (2004), Assimilation of the 2000–2001 CO MOPITT retrievals with optimized surface emissions, *Geophys. Res. Lett.*, *31*, L20105, doi:10.1029/2004GL021037.

Zbinden, R. M., V. Thouret, P. Ricaud, F. Carminati, J.-P. Cammas, and P. Nédélec (2013), Climatology of pure tropospheric profiles and column contents of ozone and carbon monoxide using MOZAIC in the mid-northern latitudes (24° N to 50° N) from 1994 to 2009, *Atmos. Chem. Phys.*, *13*, 12,363–12,388.

Zeng, G., S. W. Wood, O. Morgenstern, N. B. Jones, J. Robinson, and D. Smale (2012), Trends and variations in CO, C_2H_6, and HCN in the Southern Hemisphere point to the declining anthropogenic emissions of CO and C_2H_6, *Atmos. Chem. Phys.*, *12*, 7543–7555, doi:10.5194/acp-12-7543-2012.

Zoogman, P., D. J. Jacob, K. Chance, H. M. Worden, D. P. Edwards, and L. Zhang (2014), Improved monitoring of surface ozone air quality by joint assimilation of geostationary satellite observations of ozone and CO, *Atmos. Environ.*, *84*, 254–261.

Zubrow, A., L. Chen, and V. R. Kotamarthi (2008), EAKF-CMAQ: Introduction and evaluation of a data assimilation for CMAQ based on the ensemble adjustment Kalman filter, *J. Geophys. Res.*, *113*, D09302, doi:10.1029/2007JD009267.